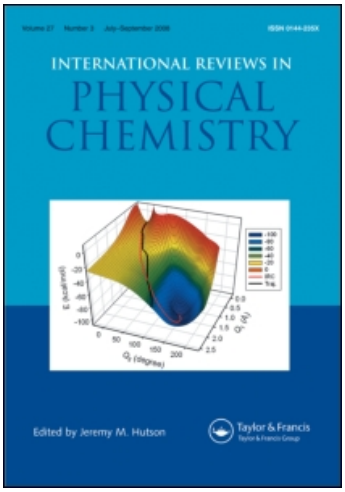

International Reviews in Physical Chemistry
Publication details, including instructions for authors and subscription information:
http://www.informaworld.com/smpp/title~content=t713724383

Proton tunnelling in polyatomic molecules: A direct-dynamics instanton approach

Willem Siebrand; Zorka Smedarchina; Marek Z. Zgierski; Antonio Fernandez-RAMOS

Online publication date: 26 November 2010

To cite this Article Siebrand, Willem , Smedarchina, Zorka , Zgierski, Marek Z. and Fernandez-RAMOS, Antonio(1999) 'Proton tunnelling in polyatomic molecules: A direct-dynamics instanton approach', International Reviews in Physical Chemistry, 18: 1, 5 — 41
To link to this Article: DOI: 10.1080/014423599229992
URL: http://dx.doi.org/10.1080/014423599229992

INTERNATIONAL REVIEWS IN PHYSICAL CHEMISTRY, 1999, VOL. 18, NO. 1, 5–41

Proton tunnelling in polyatomic molecules: a direct-dynamics instanton approach

WILLEM SIEBRAND, ZORKA SMEDARCHINA, MAREK Z. ZGIERSKI and ANTONIO FERNÁNDEZ-RAMOS

Steacie Institute for Molecular Sciences, National Research Council of Canada, Ottawa, K1A 0R6 Canada

In this review we discuss a recently introduced method of calculating hydrogen tunnelling rates and tunnelling splittings in medium and large molecules. It is a non-empirical, direct-dynamics method that uses *ab initio* quantum-chemical output as input data for the calculation of dynamic properties by means of the instanton approach. This approach is based on the recognition that there is a single path that dominates the tunnelling rate. This so-called *instanton* trajectory is the path that minimizes the classical action. Although it is very difficult to calculate this trajectory for multidimensional systems, it will be shown that the corresponding *instanton action*, which is the quantity of practical interest, can be obtained with sufficient accuracy to reproduce experimental observations without the explicit evaluation of the instanton trajectory. In this approximation scheme the instanton action is calculated from the one-dimensional action through the introduction of appropriate correction terms for all modes coupled to the tunnelling mode. These coupled transverse modes are taken to be harmonic oscillators; the couplings are assumed to be linear and derived from the displacements of the transverse modes between the equilibrium configuration and the transition state. Nonlinear couplings of large-amplitude transverse modes are also briefly discussed. The reaction coordinate is identified with the normal mode with imaginary frequency in the transition state and not with the minimum-energy path used in variational transition-state theory. The multidimensional potential-energy surface is formulated in terms of the normal coordinates of the transition state. Formulas and computer codes are presented which allow direct evaluation of mode-specific tunnelling splittings as well as of proton transfer rate constants across symmetric or asymmetric barriers as a function of temperature. Results are presented for these rates and splittings that can be critically compared with experimental data. Mode-specific splittings are discussed for 9-hydroxyphenalenone and tropolone, two large molecules for which excellent experimental data are available. Tunnelling rate constants are discussed for aziridine, oxiranyl and dioxolanyl, three medium-size molecules that undergo inversion by a tunnelling mechanism, and for porphine, a large molecule for which an abundance of high-quality proton-transfer data has been reported. All of these systems are handled successfully by the method. The calculations are performed with the DOIT (dynamics of instanton tunnelling) code, which is available on the internet. This dynamics code is very efficient compared to other available codes based on transition-state theory with tunnelling corrections and takes only a fraction of the computer time required for the computation of the quantum-chemical input data.

Contents

0144-235X/99 $12·00

1. Introduction

Proton transfer is an elementary step common to many chemical reactions, including those important in enzymatic processes. Nevertheless our understanding of the dynamics of proton transfer lags behind that of transfer of heavier nuclei, the reason being that light particles such as protons are subject to strong quantum effects and hence cannot be treated satisfactorily by classical mechanics. Most prominent among these effects is the ability of a proton to tunnel through a potential-energy barrier, thereby avoiding passage through the transition state. As a consequence, the temperature dependence of a tunnelling reaction cannot be used to measure the height of the barrier. Typically, this temperature dependence assumes the form of a curved Arrhenius plot, in which the slope of the logarithm of the rate constant plotted against the inverse temperature varies from zero for very low temperatures to a value representing the barrier height for very high temperatures. Although in the past it was often assumed that proton tunnelling was a low-temperature phenomenon that can be ignored at room tempature, it is becoming increasingly clear that tunnelling remains the prevailing mechanism of proton transfer in most temperature regions of practical interest. This follows from studies of the kinetic isotope effect. Because in the series protium, deuterium, tritium the classical character increases in proportion to the atomic weight, a strong decrease in the transfer rate or the corresponding spectral splitting upon substitution of a heavier hydrogen isotope is *prima facie* evidence for tunnelling. Such kinetic isotope effects have long been used to analyse reaction mechanisms.

Another aspect of the low atomic weight of hydrogen is the relationship between the motion of the proton and the vibrational frequencies of the heavier atoms between which the proton is transferred. Before and after transfer, the proton vibrates with a frequency that is generally high compared to these frequencies, so that vibrational averaging over the heavy-atom motions is not permitted. Unless these frequencies are so low that they can be treated classically, it will be necessary to treat the tunnelling as a multidimensional process involving many degrees of freedom. This in fact has been the greatest impediment to the development of a quantitative theory of tunnelling dynamics. It has been well recognized that one-dimensional barriers, which remain popular as a means to arrange kinetic data, are inadequate for an *ab initio* description of tunnelling dynamics. To obtain a physically relevant picture, it is necessary to include at least one other degree of freedom and, depending on the system, to add coupling to a classical heatbath. Several such treatments have been reported, based on transition-state theory [1–6], classical-trajectory calculations [7–12], the Golden Rule [13–15], or on the instanton [16–18] method. In these treatments the additional degree of freedom (or the heatbath) represents the transverse vibrations of the system by means of empirical parameters.

In this review we discuss a more ambitious method [19–26] that includes all vibrational degrees of freedom through parameters calculated by *ab initio* methods. It is based on the instanton approach. Earlier multidimensional treatments based on variational transition-state theory with semiclassical tunnelling corrections (VTST/ST) [1–6] were found to have several drawbacks that are avoided in the new approach. Thus VTST/ST requires a basically arbitrary choice between two limiting paths, an adjusted minimum-energy path (small-curvature approximation [5]) or a straight path (large-curvature approximation [6]), whereas the instanton approach is based on the correct minimum-action path. Furthermore, VTST/ST fails in the low-temperature limit, where it does not yield a temperature-independent rate constant, and it is unsuitable for the calculation of tunnelling splittings of vibrationally excited levels of transverse modes [25]. It may be argued that for temperatures of practical interest, e.g. for enzymatic reactions, VTST/ST remains satisfactory. However the VTST/ST method is very demanding in CPU time and therefore limited to relatively small systems or low-level quantum-chemical methods. The method we present is at least of equal accuracy at these temperatures and orders of magnitude more efficient. Hence it can deal successfully with large systems, the main limitation being the level of complexity that can be handled by the available quantum-chemical methods.

This method, based on the instanton approach, has been reported in a series of papers [19–26], in each of which a specific molecule or group of molecules was treated *ab initio*. It is a direct-dynamics method: the output of quantum-chemical calculations serves as direct input for the calculation of tunnelling splittings of ground and excited levels and of tunnelling rates as a function of temperature. The method is very efficient and allows treatment of systems of any size that can be handled quantum-chemically. For most purposes it requires calculation of the structure and vibrational force field in stationary points only. The dynamics calculations are performed with the DOIT (dynamics of instanton tunnelling) code [27].

In the following sections we present an introduction to instanton theory and its adaptation to multidimensional proton transfer. Before considering the instanton formalism, we introduce a novel representation of the potential-energy surface that is specially useful for proton tunnelling. The instanton formalism is presented in two parts. In the main text we provide a simplified description that emphasizes the

qualitative features of the method and in the Appendix we provide additional algebraic details. For the remainder of this review we focus on a number of applications intended to give an overall picture of our present understanding of proton tunnelling dynamics.

2. Potential-energy surfaces

To describe the transfer, we require a potential-energy surface that can be evaluated by quantum-chemical methods. The reaction of interest is the transfer of a light particle between two much heavier particles. Since the proton moves generally much faster than the atoms to which it is or becomes attached, the correct lowest-order description of the transfer process starts from a frozen skeletal structure and not from a structure that is vibrationally averaged over the skeletal vibrations. This implies that the reaction coordinate s used as the reference trajectory in variational transition-state theory [1,4], which, apart from minor modifications, amounts to the adiabatic minimum-energy path, is not a good starting point for tunnelling calculations. It is more realistic to start from a configuration in which the heavy atoms remain frozen during the transfer. Our zeroth-order approximation to the potential is therefore a one-dimensional double-minimum potential $U_C(x)$ with all atoms except the transferring proton frozen in their equilibrium positions. It is thus, according to the usual definition, a crude adiabatic rather than an adiabatic potential.

Of course this zeroth-order one-dimensional potential will be very inaccurate. It is well-recognized that heavy-atom motion can make major contributions to the tunnelling rate. This is immediately obvious for the motion that modifies the distance between the atoms carrying the hydrogen before or after the transfer. It is also supported by direct experimental observations, such as the dependence of tunnelling splittings on the excitation of skeletal vibrations [28,29]. A more subtle confirmation comes from the observation that in some tunnelling reactions the zero-temperature limit is reached at almost the same temperature for deuterium as for hydrogen [30], which shows that this temperature is determined by non-hydrogenic low-frequency skeletal modes. To generate an appropriate multidimensional potential, we unfreeze the transverse modes and treat them as harmonic oscillators. In this picture the (mass-weighted) reaction coordinate x remains associated with the proton motion and should not be confused with the minimum-energy path used as the reaction coordinate s in transition-state theory.

2.1. *Symmetric barriers*

To define the coordinate x more precisely, we first consider symmetric potentials and note that some of the transverse modes can undergo displacements if we move from the transition state, taken to be $x = 0$, to the equilibrium configurations $x = \pm\Delta x$, namely the modes that are either symmetric or antisymmetric with respect to the dividing plane through the transition state. Denoting the transverse coordinates collectively by $\mathbf{y}$, we use subscripts s and a to single out these symmetric and antisymmetric coordinates. Their displacements between the transition state and the equilibrium configuration are denoted by Δy_s and $\pm\Delta y_a$, respectively. Modes that are asymmetric but not antisymmetric cannot be displaced and are expected to play a minor role; these modes, to be labelled by a subscript b, will be considered later in this section.

It will turn out that for our purpose the effect of transverse modes on the

tunnelling dynamics is basically additive, each coupled mode making its own contribution [19]. As a first approximation we therefore ignore mixing of the transverse modes during the tunnelling; we also neglect frequency changes, and restrict ourselves to linear couplings with the reaction coordinate. These couplings relate the displacements $\Delta y_{a,s}$ to Δx and can be written in the form

$$C_{a,s} = \omega_{a,s}^2 \Delta y_{a,s} / \Delta x, \tag{1}$$

where $\omega_{a,s}$ represent the transverse-mode frequencies. The multidimensional potential then assumes the form

$$U(x, \mathbf{y}) = U_C(x) + \tfrac{1}{2} \sum_{a,s} \omega_{a,s}^2 (y_{a,s}^2 - \Delta y_{a,s}^2) - |x| \sum_s C_s (y_s - \Delta y_s) - x \sum_a C_a (y_a \pm \Delta y_a), \tag{2}$$

where $\tfrac{1}{2} \sum_{a,s} \omega_{a,s}^2 \Delta y_{a,s}^2$ represents the relevant contribution to the reorganization energy. To avoid the singularity at $x = 0$ of the term proportional to $|x|$, we use the replacements $|x| \rightarrow x^2$, $C_s \rightarrow C_s / \Delta x$, which yields results equivalent to those of equation (2). For simplicity we omit for the time being terms of the form $\omega_b^2 y_b^2 / 2$ corresponding to modes that are not linearly coupled to the transfer mode and thus do not contribute in this approximation.

In practice, it is more convenient to use an adiabatic formulation, since the quantum-chemical results are produced in this form. To obtain the adiabatic potential, we set $\partial U(x, \mathbf{y}) / \partial y_{a,s} = 0$, which yields

$$U_a(x) = U_C(x) - \tfrac{1}{2} (1 - |x| / \Delta x)^2 \sum_{a,s} (\omega_{a,s} \Delta y_{a,s})^2, \tag{3}$$

leading to an adiabatic potential of the form

$$U(x, \mathbf{y}) = U_a(x) + \tfrac{1}{2} \sum_a \omega_a^2 (y_a - x C_a / \omega_a^2)^2 + \tfrac{1}{2} \sum_s \omega_s^2 (y_s - |x| C_s / \omega_s^2)^2. \tag{4}$$

The transition state is the only configuration where the reaction coordinate coincides exactly with a (generalized) normal mode, namely the mode with imaginary frequency. It is also the configuration of highest symmetry. Therefore we choose it as the origin of the vibrational coordinates, i.e. we measure all displacements Δx and $\Delta y_{a,s}$ relative to this structure. Thus near the top of the barrier, where $x \simeq 0$ and

$$U_a(x) \simeq U_0 - \tfrac{1}{2} (\omega^* x)^2, \tag{5}$$

we have

$$U_{x \rightarrow 0}(x, \mathbf{y}) \simeq U_0 - \tfrac{1}{2} (\omega^* x)^2 + \tfrac{1}{2} \sum_{a,s} (\omega_{a,s} y_{a,s})^2, \tag{6}$$

where U_0 is the adiabatic barrier height and ω^* the adiabatic imaginary frequency in the transition state. From these equations it follows that the reaction coordinate x near its origin is the normal mode with imaginary frequency and that the coupled transverse modes $y_{a,s}$ are other normal modes in the transition state. Similarly, we have near the minimum, where $x \simeq \pm \Delta x$,

$$U_a(x) \simeq \tfrac{1}{2} \Omega_0^2 (x \pm \Delta x)^2, \tag{7}$$

so that

$$U_{x \rightarrow \pm \Delta x}(x, \mathbf{y}) \simeq \tfrac{1}{2} \Omega_0^2 (x \pm \Delta x)^2 + \tfrac{1}{2} \sum_a \omega_a^2 (y_a \pm \Delta y_a)^2 + \tfrac{1}{2} \sum_s \omega_s^2 (y_s - \Delta y_s)^2, \tag{8}$$

where Ω_0 is an effective harmonic frequency associated with the reaction coordinate x in the equilibrium configuration.

To calculate this frequency we have to consider the mixing of vibrational modes that will take place between the equilibrium configuration and the transition state. The actual normal coordinates of the equilibrium configuration, to be denoted collectively by $\mathbf{z}$, will be different from the set $x, \mathbf{y}$ and lead to a potential of the form

$$U_{\mathrm{eq}}(\mathbf{z}) = \tfrac{1}{2}\sum_j \omega_j^2(z_j \pm \Delta z_j)^2 + \tfrac{1}{2}\sum_k \omega_k^2(z_k - \Delta z_k)^2, \tag{9}$$

where j and k run over the modes that are, respectively, displaced and not displaced between the minima, with displacements $\Delta z_{j,k}$ relative to the transition state. In addition there will be terms $\frac{1}{2}\omega_n^2 z_n^2$ corresponding to modes that are not displaced between the transition state and the equilibrium configuration. The coordinates $\mathbf{z}$ can be related to the coordinates $x, \mathbf{y}$ by a unitary matrix $\mathbf{G}$, which separates into three blocks, G_{aj}, G_{sk} and G_{bn}, the last block referring to modes without linear coupling. These transformations must be carried out in such a way that the Eckart conditions [31] are met, so that no mixing with rotations occurs. The $\mathbf{G}$ matrix allows us to calculate the effective frequency of the transfer mode in the equilibrium configuration:

$$\Omega_0^2 = \sum_j G_{0j}^2 \omega_j^2, \tag{10}$$

where $x = \sum_j G_{0j} z_j$ and $\sum_j G_{0j}^2 = 1$. Equations (7) and (10) describe the reaction coordinate x in the equilibrium configuration.

In general we transform calculated interatomic distances into vibrational displacements through the relation [19]

$$\Delta(x, \mathbf{y}) = \mathbf{r}\cdot\mathbf{L}, \tag{11}$$

where $\mathbf{r}$ is the vector of the mass-weighted atomic displacements between the transition state and the equilibrium configuration and $\mathbf{L}$ is the $3N \times (3N - 6)$ matrix that relates the normal coordinates of the transition state to the mass-weighted Cartesian coordinates of the atoms. For values of x intermediate between 0 and $\pm\Delta x$, we obtain the corresponding structure through the relations

$$\partial U_A(x, \mathbf{y})/\partial \mathbf{y} = \mathbf{0} \tag{12}$$

and compute the energy by single-point calculations.

In general mixing of the transverse modes among themselves is expected to have a minimal effect on zero-point splittings and on the temperature dependence of tunnelling rate constants, because these effects represent the positive and negative contributions of many modes, which should roughly average out because of the unitarity of $\mathbf{G}$. However, this mixing may become important for mode-specific rate constants and splittings. For each excited mode j we must then determine the contributions G_{aj}^2 and G_{sk}^2 of the corresponding modes y_a and y_s to the rate or the splitting (see below).

The present formulation of the potential-energy surface, given by equation (4), differs from that used in the approach to tunnelling derived from variational transition-state theory, which uses the reaction-path Hamiltonian. In that Hamiltonian the reaction coordinate is the minimum-energy path rather than a normal coordinate, so that the couplings to the transverse modes enter via the kinetic-energy

operator. In our formulation the kinetic-energy operator remains diagonal and the couplings enter via the potential. The problem with the reaction-path Hamiltonian applied to proton transfer is that the required effective integration over the transverse-mode coordinates is very difficult unless these modes are treated in the adiabatic approximation. Although the corresponding vibrational averaging is generally appropriate for modes with frequencies higher than the tunnelling frequency, the coupled modes for proton transfer are typically low-frequency modes. In practice, one therefore tends to replace the resulting tunnelling trajectory by the *ad hoc* assumption of a straight-line path [6], an approach that is computationally very inefficient and tends to be inadequate for dealing with isotope effects. In our formulation of the potential-energy surface, the couplings enter as potential-energy terms that are linear in the transverse-mode coordinates. It will turn out [18] to be possible to integrate analytically over these coordinates without invoking the adiabatic approximation.

2.2. *Asymmetric barriers*

So far we have only considered symmetric transition states. In our approach the effect of the couplings to the reaction coordinate depends on the symmetry of the transverse modes, which is lost for asymmetric barriers. However, we can still recognize modes that can be classified as basically symmetric and basically antisymmetric with respect to the dividing surface of the transition state. To make use of this, we separate each mode into its 'symmetric' and 'antisymmetric' components by associating the symmetric component with the sum of the displacements from the transition state to the initial and final states, and the antisymmetric components with their difference:

$$\Delta y_m^{s,a} = \tfrac{1}{2}(y_m^{\mathrm{f}} \pm y_m^{\mathrm{i}}), \tag{13}$$

where the superscripts 'i' and 'f' denote the initial and final equilibrium configurations, respectively. This approach relates the mixing of symmetric (+) and antisymmetric (−) components to the barrier asymmetry and reduces to the earlier expressions if the barrier is symmetric. Combined with the definition $\Delta x = (x^{\mathrm{f}} - x^{\mathrm{i}})/2$, this allows us the retain the form of the potential $U(x, \mathbf{y})$ given by equation (4) provided we replace the coordinates $y_{a,s}$ by their components $y_m^{a,s}$.

Since the two wells have different energies in the case of an asymmetric barrier, there are two different rate constants, depending on which well corresponds to the initial state. According to the principle of microscopic reversibility, these rate constants differ by a Boltzmann factor $\exp(\Delta E / k_{\mathrm{B}} T)$, where ΔE is the energy difference between the initial and the final well.

2.3. *The barrier along the reaction coordinate*

To evaluate the one-dimensional adiabatic tunnelling potential $U_A(x)$, we use quantum-chemical methods for the stationary points and as many additional points as required to obtain the desired accuracy. For symmetric potentials, the stationary points produce four parameters relevant to the generation of the barrier, namely the displacement Δx, the barrier height, and the curvatures at the top and the bottom of the barrier, from which a potential can be generated by interpolation. In simple cases it may be sufficient to use an analytical interpolation scheme. For instance, to calculate tunnelling splittings, one may only need an accurate representation of the barrier shape in the bottom region. In that case a two-parameter quartic expression

of the form

$$U_A(x) \approx U_q = U_0[1 - (x/\Delta x)^2]^2, \tag{14}$$

where U_0 and Δx are the calculated barrier height and reaction-coordinate displacement, respectively, may be satisfactory. To add a third parameter, one can modify the curvature at the bottom of the potential by a shape function, e.g.

$$U_A(x) \approx U_q(1 + A \exp[-B(x^2 - \Delta x^2)^2]). \tag{15}$$

If all four calculated parameters are to be used, these analytical potentials are not practical; in that case a direct interpolation scheme is to be preferred.

These analytical potentials can be adapted to asymmetric barriers by addition of a cubic term. In that case there will be two additional parameters produced by the stationary point calculations, namely the energy and the curvature of the final state. In principle it is possible to use the method of equation (12) to calculate parameters for intermediate points, but this procedure requires further testing.

3. Instanton method

Proton tunnelling rates depend exponentially on the tunnelling distance. Since potential-energy barriers tend to get narrower near the top, tunnelling rates also depend exponentially on the energy of the tunnelling proton. These exponential dependences tend to put strong restrictions on the effective tunnelling trajectories. The instanton approach is based on the recognition that these restrictions give rise to a dominant tunnelling trajectory, the instanton path [16–18, 32–35]. That such a preferred trajectory exists can be inferred from the competitive nature of the distance and energy dependences: paths near the bottom of the barrier require little energy but imply long tunnelling distances, whereas paths near the top correspond to short tunnelling distances but require more energy. The (temperature-dependent) instanton trajectory is the most favourable compromise between these conflicting requirements and dominates the transfer below the top of the barrier. In this section we restrict ourselves to a qualitative introduction to the instanton formalism; mathematical details can be found in the Appendix.

3.1. *One-dimensional potentials*

To illustrate the nature of the instanton path, we start with a one-dimensional potential $U(x)$, for which the instanton reduces to a familiar form in terms of the classical action (here and hereafter we use units $\hbar = 1$)

$$S_C(E) = \int_{x_1}^{x_2} dx \{2[U(x) - E]\}^{1/2}, \tag{16}$$

where x_1 and x_2 are the classical turning points for energy E. The corresponding transfer rate constant is given by the well-known expression [35, 36]

$$k(T) = Z_0^{-1} \int_0^\infty dE \exp[-2S_C(E)] \exp(-\beta E), \tag{17}$$

where $\beta = 1/k_B T$ and $Z_0 = \sum_n \exp(-E_n\beta)$ is the partition function for the initial state. For temperatures where tunnelling dominates, we can use the method of steepest descent to find the trajectory that dominates the integral, so that we can carry out the integration. This *instanton path* is characterized by a value $\tau = \beta$ for the period of the classical motion in the upside-down potential $-U(x)$ [16].

The instanton action along this path, $S_I^0(T)$, equals twice the classical action. The integration reduces equation (17) to

$$k(T) = A^0(T) \exp[-S_I^0(T)], \tag{18}$$

where $A^0(T)$ represents a distribution of channels centred about the instanton path as required to make the transition irreversible.

3.2. *Multidimensional potentials*

The simple form of equation (18) is due to the existence of a dominant path. To show that the same form applies to multidimensional tunnelling, we have to demonstrate that in that case there is a preferred path as well. As shown in the Appendix, this demonstration makes use of path integrals [37] describing closed trajectories in imaginary time in the upside-down potential $-U(x, \mathbf{y})$. Among these trajectories, there are periodic orbits for which the Euclidian action S_E (i.e. the action in the upside-down potential) has an extreme value, to be obtained by solving the equations $\partial S_E/\partial x = 0$ and $\partial S_E/\partial \mathbf{y} = 0$. This yields the stationary solutions corresponding to the equilibrium configurations, a saddle point corresponding to the transition state, which contributes a term $\sim \exp(-\beta U_0)$, and a second saddle point corresponding to the instanton trajectory, which contributes a term $\sim \exp[-S_I(\beta)]$. The latter term justifies the generalization of equation (18) to tunnelling rate constants in multidimensional potentials:

$$k(T) = A(T) \exp[-S_I(T)], \tag{19}$$

where S_I is the Euclidian action of the instanton path. From its definition as a periodic orbit in the upside-down potential it follows that the shortest possible instanton path, corresponding to the temperature where tunnelling occurs just below the top of the barrier, will be the zero-point amplitude of this potential. This defines the cross-over temperature $T^* = \omega^*/2\pi k_B$ above which the transfer occurs classically, since the transfer rate constant (17) will then be governed by the saddle point corresponding to the transition state.

This leaves us with the problem of determining the instanton path. The corresponding extreme-value equations lead to as many coupled equations of motion as there are vibrational degrees of freedom; in practice this means that it is very difficult to find exact solutions for more than two dimensions [17, 18]. To deal with large systems, approximations will be unavoidable. To find suitable approximations, we first consider a simple two-dimensional model studied by Benderskii *et al.* [38]. It consists of two crossing harmonic potentials, $U(x)$ in our notation, coupled to a totally symmetric harmonic vibration y_s. This problem can be solved exactly and allows straightforward generalization to several coupled totally symmetric vibrations. The resulting expression for the multidimensional instanton action as a function of temperature we rewrite so as to separate terms referring to the one-dimensional potential $U(x)$, which determine the one-dimensional instanton action S_I^0, from terms referring to the couplings, which provide a multidimensional correction. This correction turns out to be independent of the shape of $U(x)$. We then make the reasonable assumption that this result is valid not only for the model of two crossing harmonic potentials but for any well-behaved double-minimum potential $U(x)$. Antisymmetric vibrations are included through Franck–Condon factors; they simply add a term to

the instanton action. The final result for the action is of the form [25,26].

$$S_{\mathrm{I}}(T) = \frac{S_{\mathrm{I}}^{0}(T)}{1 + \sum_s \delta_s(T)} + \alpha_s \sum_a \delta_a(T), \tag{20}$$

where the α and δ terms are functions of the couplings C_a and C_s displayed in equations (1)–(4) (see below). For the calculation of tunnelling splittings we use the same equation in the limit $T = 0$.

A major advantage of this scheme is that explicit evaluation of the instanton trajectory is avoided. The only parameters needed for the tunnelling calculations are those governing the one-dimensional potential $U_a(x)$ and the couplings, and these can be evaluated readily by standard quantum-chemical methods. The method is not limited to rate constants but can also be used to calculate tunnelling splittings of ground and excited vibrational levels, as we shall show presently. Of course, the method is approximate and its accuracy needs to be tested by comparison with experiment. As we shall demonstrate, the tests carried out so far indicate that for large systems the method is superior in accuracy and speed to other available methods.

3.3. *Linear couplings*

To carry out the calculations, we need expressions for the parameters δ and α, associated with the coupling. For the derivation of these parameters we refer to the original literature [25,26,38]; here we simple quote the results. The correction terms for symmetric coupling in the general case of an asymmetric barrier take the form

$$\delta_s(T) = \delta_s(0) \coth \frac{\omega_j}{2k_{\mathrm{B}}T}, \tag{21}$$

where $\delta_s(0)$ is the zero-level correction term; for modes $\omega_m \ll \Omega_0$, which generally dominate the coupling, it is given by [19,23]

$$\delta_s(0) = \tfrac{1}{4}(\Omega_0/\omega_m)(C_m^s \Delta x/\Omega_0{}^2)^2, \tag{22}$$

Ω_0 being the effective frequency of the transfer mode in the initial state. The corresponding terms $\delta_a(T)$ for antisymmetric coupling depend on the asymmetry of the potential. For small asymmetry we have [26]

$$\delta_a(T) = 2(\Delta y_m^a)^2/a_{0m}^2 \coth \frac{\omega_m}{4k_{\mathrm{B}}T}, \tag{23}$$

and for large asymmetry, where the final state acts as an absorbing wall [17,18], we have instead

$$\delta_a(T) = (\Delta y_m^a)^2/a_{0m}^2 \coth \frac{\omega_m}{2k_{\mathrm{B}}T}, \tag{24}$$

$a_{0m} = \omega_m^{-1/2}$ being the zero-level amplitude of the mode y_m. At high temperatures both expressions turn into the usual activation term $\delta_a(T) = U_a/k_{\mathrm{B}}T$, where $U_a = \omega_m^2(\Delta y_m^a)^2/2$ represents the barrier height corresponding to the final reorganization of this mode. For symmetric barriers Δy_m^a reduces to Δy_a.

The factor α_s, which enters because the effect of antisymmetric coupling is modulated by symmetric couplings, assumes the form [38]

$$\alpha_s = (1 - q/2^{1/2} + q^2/4)^2, \tag{25}$$

where

$$q = R/(1 - B),$$
$$R = \sum_m (\Delta y_m^s)^2 \omega_m^3 / 2^{1/2} U_0 \Omega_0,$$
$$B = \sum_m (\Delta y_m^s)^2 \omega_m^2 / 2U_0, \tag{26}$$

the sum running over the modes with frequencies $\omega_m \ll \Omega_0$.

In the case of hydrogen transfer, one is unlikely to encounter strongly coupled modes $\omega_m \geqslant \Omega_0$. If they do occur, they couple adiabatically and their effect can be included by the introduction of an effective mass of the tunnelling particle in equation (16):

$$S_C(E) = \int_{x_1}^{x_2} dx \{2m_{\text{eff}}[U(x) - E]\}^{1/2}, \tag{27}$$

where [38]

$$m_{\text{eff}} = 1 + \sum_a (C_a/\omega_a^2)^2 + 4x^2 \sum_s (C_s/\omega_s^2)^2. \tag{28}$$

3.4. *The zero-temperature limit*

At $T = 0$ the rate constant has a non-zero limit [39]

$$k(0) = (\Omega_0/2\pi) \exp[-S_I(0)], \tag{29}$$

where the instanton action at zero-temperature is represented by

$$S_I(0) = \frac{2S_C(\Omega_0/2)}{1 + \sum_s \delta_s(0)} + \alpha_s \sum_a \delta_a(0), \tag{30}$$

$S_C(\Omega_0/2)$ being the classical action for the zero-point energy level in the initial state. This is the form used to calculate zero-point tunnelling splittings for symmetric potentials:

$$\Delta(0) = (\Omega_0/\pi) \exp[-S_I(0)/2]. \tag{31}$$

The pre-exponential factor in this equation rests on a simplifying assumption made to calculate the factor $A(T)$ in equation (19). The assumption, which we also use for the calculation of rate constants, is that the strongly coupled modes are close to the adiabatic limit. Then $A(T)$ can be replaced by $\Omega_0/2\pi$, provided the one-dimensional instanton action S_I^0 is evaluated for the vibrationally adiabatic barrier, i.e. the adiabatic barrier with the zero-point energy included [18, 38]. In that case equation (19) assumes the simple form

$$k(T) = (\Omega_0/2\pi) \exp[-S_I(T)], \tag{32}$$

where $S_I(T)$ is given by equation (20) with $S_I^0(T)$ calculated for the vibrationally adiabatic potential. Note that such an adiabatic approximation would not be valid for S_I itself, since it enters via an exponent.

3.5. *Mode-specific tunnelling splittings*

In the instanton method, as opposed to transition-state theory, it is straightforward to calculate the tunnelling splittings of vibrationally excited levels [20, 22, 24, 25]. The correction terms associated with these levels with a quantum number v in the

transition state take the simple form

$$\delta_s(v_s) = (2v_s + 1)\delta_s(0), \qquad \delta_a(v_a) = 2\delta_a(0)/(2v_a + 1). \tag{33}$$

To calculate the (observable) splitting of a level $v_{j,k}$ in the equilibrium configuration, we must use the **G** matrix:

$$v_{a,s} = \sum_{j,k} G^2_{a,s;j,k} v_{j,k}. \tag{34}$$

It follows from equation (33) that in general excitation of symmetric vibrations will increase the tunnelling splitting, whereas the effect of exciting an antisymmetric vibration depends on the magnitude of the displacement relative to a_0, the zero-level amplitude. If $\Delta y_a / a_0 \geqslant 1$, the Franck–Condon contribution of the v_ath level equals $\exp[-\alpha_s \delta_a(v_a)]$ and if $\Delta y_a / a_0 < 1$ it takes the form

$$F_a(v_a) = |L_v[\alpha_s \delta_a(0)]| \exp[-\alpha_s \delta_a(0)], \tag{35}$$

where L_v is the vth Laguerre polynomial. According to equation (31), the tunnelling splitting is proportional to the square root of this Franck–Condon factor. For a level in the equilibrium configuration excited by a single quantum of mode j, associated with antisymmetric modes a in the transition state, equation (35) can be usually approximated by

$$F_a(1_j) = [1 - \alpha_s \delta_a(0) G^2_{aj}] \exp[-\alpha_s \delta_a(0)], \tag{36}$$

where we have neglected the off-diagonal elements. It is important, however, to include mixing with the reaction coordinate, since this increases the energy at which the tunnelling occurs by an amount $\sum_j G^2_{0j} v_j$, so that the energy E in equation (16) is now given by

$$E = (v_0 + \sum_j G^2_{0j} v_j + \tfrac{1}{2})\Omega_0, \tag{37}$$

where v_0 is the quantum number of the tunnelling mode in the equilibrium configuration.

Finally we point out that the approach described here is not limited to tunnelling splittings but can also be used to evaluate mode-specific tunnelling rate constants.

3.6. *Nonlinear couplings*

So far we have limited ourselves to couplings that are linear in the transverse-mode coordinates, the assumption being that for displaced modes the lowest-order coupling terms are likely to be dominant. It has been observed, however, that modes that are not displaced and thus do not contribute to the linear coupling can still effect the tunnelling [20, 22, 24, 28]. For instance in tropolone, which remains planar during intramolecular proton transfer, excitation of low-frequency out-of-plane modes affects the tunnelling splitting. These nonlinear couplings correspond to anharmonic terms in the potential and can be positive or negative. In general the quantum-chemical methods presently available cannot reliably evaluate such terms for polyatomic molecules.

The experiments discussed in the next section suggest that nonlinear couplings are most important for low-frequency modes with large amplitudes. The effect of anharmonic coupling with high-frequency modes will be difficult to observe unambiguously because there is expected to be strong cancellation between positive and negative contributions. However, if the linear coupling with a particular mode

is very strong, one may reasonably expect nonlinear coupling to be significant for that mode. This strong-coupling case remains to be investigated.

Here we limit ourselves to low-frequency out-of-plane vibrations in planar molecules for which the lowest-order anharmonic coupling terms are of the form $x^2 \sum_b D_b y_b^2$. Whether such terms will help or hinder tunnelling depends on their sign, as can be readily verified for quartic potentials of the form (14), where they contribute to the quadratic terms. The effect of this coupling with a given mode b on the barrier height and tunnelling distance can be represented by the replacements

$$\begin{aligned} U_0 &\longrightarrow U_0[1 - (D_b/2U_0)\Delta x^2 y_b^2]^2 \\ \Delta x &\longrightarrow \Delta x[1 - (D_b/2U_0)\Delta x^2 y_b^2]^{1/2}. \end{aligned} \tag{38}$$

Thus for $D_b < 0$, both the barrier height and the tunnelling distance increase with increasing $|y_b|$, so that tunnelling will be hindered, the more so, the higher mode b is excited. For $D_b > 0$, the opposite holds, i.e. tunnelling will be helped.

Since it is not possible to integrate over nonlinearly coupled coordinates in the manner used for linearly coupled coordinates $y_{a,s}$, we cannot treat anharmonic coupling on the same level as linear coupling. However, since the anharmonically coupled modes of interest are low-frequency modes, we can treat them adiabatically. Thus we can add the anharmonic coupling terms $D_b x^2 y_b^2$ directly to the vibrationally-adiabatic potential. Using the **G** matrix, we transform to coordinates y_n of the equilibrium configuration, which we treat as parameters. We first calculate y_n-dependent splittings or rate constants and then average the result over the probability that the coordinate of mode n will have a value y_n. For instance for the vth level of the mode we find the tunnelling splitting from

$$\Delta_n(v) = \int \Delta_n(y_n)|\chi_v(y_n)|^2 \, \mathrm{d}y_n, \tag{39}$$

where $\chi_v(y_n)$ is the appropriate harmonic-oscillator wavefunction. For rate constants, averaging over y_n requires summation over the populations of the levels of mode n, which for harmonic oscillators yields the probability

$$P(y_n) = \frac{\exp\{-y_n^2/[a_{0n}^2 \coth(\omega_n/2k_\mathrm{B}T)]\}}{\int \exp\{-y_n^2/[a_{0n}^2 \coth(\omega_n/2k_\mathrm{B}T]\} \, \mathrm{d}y_n}, \tag{40}$$

where a_{0n} is the zero-point amplitude of mode n. The rate constant then assumes the form

$$k(T) = \int \ldots \int k(y_{\ldots n \ldots}) \prod_n P(y_{\ldots n \ldots}) \, \mathbf{d}y_{\ldots n \ldots}. \tag{41}$$

4. Comparison with experiment

Since the theory outlined in the preceding sections contains many approximations, the limits of its applicability and its accuracy within these limits need to be established by comparison with experiment. The comparisons to be discussed concern both tunnelling splittings and rate constants. To test the applicability of the dynamics, we need to consider properties that do not rely critically on the accuracy of the quantum-chemical input data. Thus zero-point level splittings or rate constants measured at a single temperature are unsuitable given their sensitivity to calculated barrier heights. Of more interest are kinetic isotope effects, especially if they are observed for all three hydrogen isotopes. The most useful data are those

that combine isotope effects with temperature dependences for rate constants and with mode-specific splittings for spectra.

The calculations are performed with our D(ynamics) O(f) I(nstanton) T(unnelling) program, which was recently made available via the internet [27]. This is direct-dynamics code, to be used in conjunction with a suitable quantum-chemistry code. The calculations reported here used the GAUSSIAN92 or 94 suites of programs [40] to calculate optimized geometries, vibrational force fields and tunnelling barriers. Note that the one-dimensional barrier used in the calculation of the instanton action is the vibrationally adiabatic barrier. The main decision to be made about the quantum-chemical part of the calculation is, apart from the choice of the level of theory and the basis set, the approach to be adopted to establish the shape of the barrier. Since it is notoriously difficult to calculate accurate barrier heights for large systems in general and for hydrogen-bonded systems in particular, the most effective strategy is often to restrict the calculations to the stationary points along the minimum-energy path, transform to the reaction coordinate x by the method outlined in section 2 and use an interpolation scheme to connect the resulting points, taking into account that in most cases the barrier height will require empirical adjustment. The latter problem is not specific to our instanton approach but affects all dynamics calculations. While it seriously interferes with our ability to deal with single data points, it is much less serious when extensive sets of data are available, so that one can compare ratios of splittings and rate constants rather than rely on their absolute values.

4.1. *Tunnelling splittings*

First we consider tunnelling splittings. Accurate mode-specific splittings are available for two large molecules, tropolone [41] and 9-hydroxyphenalenone (9HPO) [29,42], illustrated in figure 1. In both molecules the proton exchange is between a keto and an enol group; in tropolone the keto and enol carbons are adjacent and form part of a planar olefinic ring, while in 9HPO they are separated by a third carbon atom and are part of a condensed aromatic ring system. The active site in 9HPO is the same as that in malonaldehyde [21,43–49], also depicted in figure 1, but for this simpler molecule, to which we return in the next section, no mode-specific data are available. This is regrettable since the structure of malonaldehyde is known accurately [50,51] and can serve as a test for the quantum-chemical structure calculations to be used for the dynamics. Applied to the calculations reported thus far [21,46], this test indicates that it is very difficult to obtain an accurate representation of the hydrogen-bonded structure by standard Hartree–Fock and density-functional methods. By the same token one expects the calculated energetics of the transfer to be subject to considerable uncertainty, so that the absolute values of the splittings cannot be used to probe the dynamics methodology. Instead we shall focus on observations such as the isotope effect and the effect of exciting specific transverse modes.

4.1.1. *9-Hydroxyphenalenone*

In 9HPO the transfer takes place in a six-membered ring structure. Mode-specific splittings in the ground state of the mono-deuterio isotopomer (9DPO) have been measured in a cold beam [29,42]. For 9HPO itself only the zero-point splitting has been observed since this splitting proved too large for thermal population of the upper level, thus inhibiting the observation of mode-specific splittings. The structure

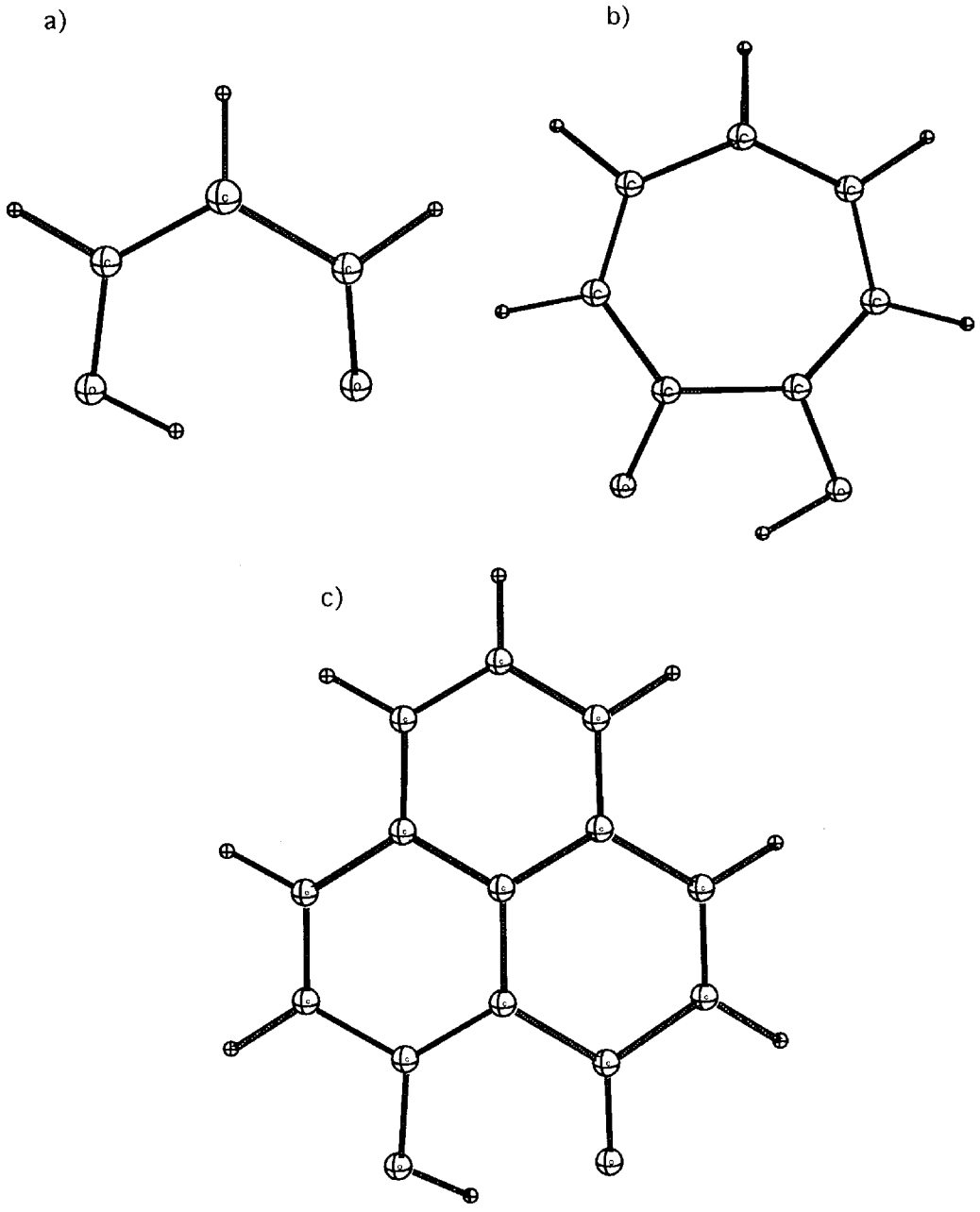

Figure 1. (*a*) Malonaldehyde, (*b*) tropolone and (*c*) 9-hydroxyphenalenone.

and force field were calculated at the HF/6-31G** level, and the quartic potential (14) was used to interpolate between the stationary configurations [25]. Two transition-state modes are strongly displaced: a symmetric mode of 745 cm^{-1}, correlated with mode 1 (288 cm^{-1}) and mode 8 (629 cm^{-1}), and an antisymmetric mode of 504 cm^{-1}, correlated with mode 5 (429 cm^{-1}) in the equilibrium configuration.

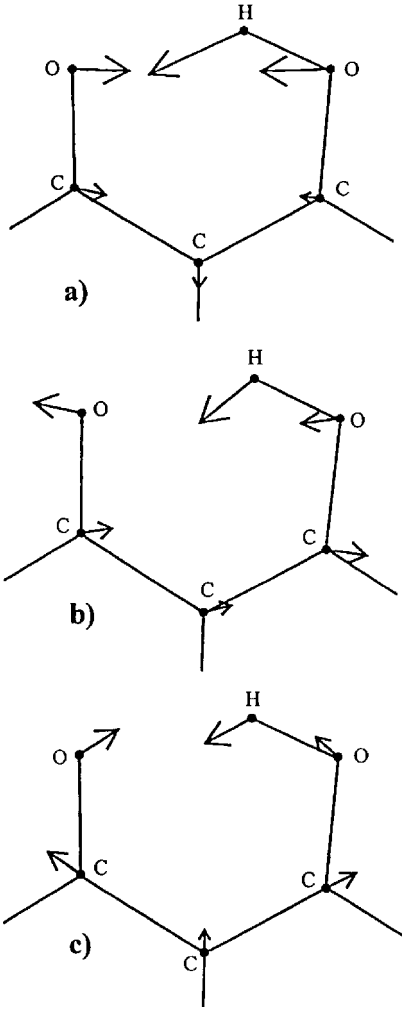

Figure 2. Three transverse modes of 9-hydroxyphenalenone that are strongly coupled to the transfer mode: (*a*) $\omega_1^0 = 288\,\mathrm{cm}^{-1}$, (*b*) $\omega_5^0 = 429\,\mathrm{cm}^{-1}$, and (*c*) $\omega_8^0 = 629\,\mathrm{cm}^{-1}$.

The calculations produced low values for the zero-point splitting. This is ascribed to inaccurate quantum-chemical input data, based in part on our previous experience that the Hartree–Fock method tends to produce barriers that are too high and in part on the fact that the VTST/ST large-curvature approximation based on the same input data yields roughly the same low zero-point splitting. While it is possible that both the tunnelling distance and the barrier height are predicted inaccurately, we have restricted ourselves to scaling the calculated barrier height by a factor 0.87 to $2658\,\mathrm{cm}^{-1}$ or $7.6\,\mathrm{kcal\,mol}^{-1}$. This yields correct zero-point splittings for both 9HPO and 9DPO, and hence the correct isotope effect (for the same barrier the VTST/ST method also yields the correct zero-point splitting for 9HPO, but underestimates the splitting for 9DPO [25]). Therefore the scaled barrier was used to calculate the mode-specific splittings.

Splittings have been reported for five excited levels corresponding to three modes,

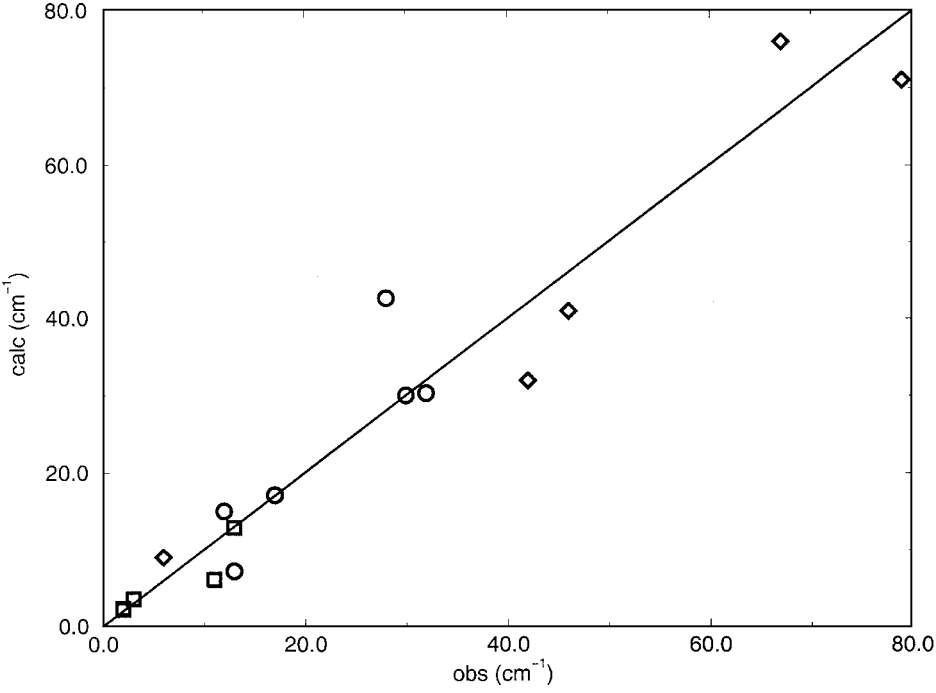

Figure 3. Comparison of calculated and observed mode-specific splittings in tropolone (circles), tropolone-d_1 (squares), and 9-hydroxyphenalenone-d_1 (diamonds).

two symmetric (ω_1 and ω_8) and one antisymmetric (ω_5); they are the modes with the strongest calculated displacements depicted in figure 2. As predicted by theory, the symmetric modes along with their overtones and combinations enhance the splitting, whereas the antisymmetric mode reduces it [25]. The correlation between the calculated and observed splittings is depicted graphically in figure 3. Although the agreement is not perfect, it convincingly demonstrates the effect of coupling to transverse modes on the splitting.

4.1.2. *Tropolone*

Similar calculations have been carried out for tropolone, where the transfer occurs in a five-membered ring, which is more strained than the six-membered ring of 9HPO and leads to a much smaller splitting. In the ground state, the splitting has only been measured for the zero-point level and, with some uncertainty, for the OH-stretch mode [52], but mode-specific splittings have been observed [41] in the lowest singlet-excited state for both tropolone-d_0 and tropolone-d_1. As for 9HPO, some of these splittings were found to be smaller and others were found to be larger than the zero-point splitting.

The excited-state calculations were carried out at the CIS/6-31G** level and again the quartic potential (14) was used to interpolate between the stationary points [22]. In parallel calculations on the electronic ground state it was found that the barrier height is very sensitive to the method of calculation, with B3LYP/6-31G** and MP2/6-31G** showing a much lower barrier than HF/6-31G** and certainly too low to explain the observed small zero-point splitting of 1 cm^{-1}. We

therefore used the HF and CIS approaches for the ground state and the excited state, respectively, scaled so as to reproduce the observed zero-point splittings of 0.99 and 18.9 cm^{-1}. The corresponding scaling factors of 0.9 and 0.68, respectively, yield barrier heights of 4930 and 2840 cm^{-1}. The latter barrier also reproduced the observed splitting of 2 cm^{-1} in the mono-deuterio isotopomer.

The only mode for which the tunnelling splitting in the ground state has been reported is the OH-stretch vibration which is the main component of the transfer mode, and hence strongly dependent on the form of $U_a(x)$. For simplicity, we have used the quartic potential, but applied a correction deduced from the analogy with malonaldehyde. Specifically, we have introduced anharmonicity constants of $-300/-220$ cm^{-1} for tropolone-H/D to correct the zero-point energy. The calculated splittings of 15/0.8 cm^{-1} are to be compared with the reported value of 12 cm^{-1} for the H isotopomer.

In the excited state, three transition-state modes were found to be strongly displaced, namely two symmetric modes of 2002 (1456 in d_1) and 734 cm^{-1}, and one antisymmetric mode of 549 cm^{-1}. Since the observed spectrum does not extend much beyond 700 cm^{-1}, the first of these modes does not give rise to an observable transition. The 734 cm^{-1} fundamental is a major component of mode 13 (observed/calculated 415/422 cm^{-1}) and mode 14 (298/355 cm^{-1}), both of which show enhanced splitting relative to the zero-point level. The 549 fundamental is the major component of mode 11 (511/519 cm^{-1}), which shows a reduced splitting. The remaining observed in-plane fundamentals show splittings similar to the zero-point splitting. All these observations agree with the predictions [22]. A comparison between calculated and observed splittings is shown graphically in figure 3.

However, the tropolone fluorescence excitation spectrum also shows out-of-plane fundamentals and progressions with splittings differing from the zero-point splitting. Since tropolone is planar and is calculated to remain planar in the transition state, these modes are not displaced and do not contribute to the linear coupling with the reaction coordinate. Their lowest-order contribution is quadratic in both the reaction coordinate and the out-of-plane mode coordinate and thus represents anharmonic coupling. Since the quantum-chemical programs available cannot reliably calculate anharmonicities for this molecule, we cannot extend the present *ab initio* calculation of tunnelling splittings to undisplaced modes. It is possible to account for the observed splitting by assuming an empirical anharmonic coupling, which makes sense in the case of a progression where one coupling parameter can account for a series of different splittings, but this is outside the scope of the present section, which is limited to predictions based on calculated parameters. We return to this problem in the next section.

4.1.3. *Summary of splittings*

The results obtained so far can be summarized as follows. The theory has been applied to two planar molecules of considerable complexity. It has proved effective in accounting for the splitting of in-plane fundamentals relative to the zero-point splitting. These relative splittings are calculated by *ab initio* methods from the displacements of the normal modes between the transition state and the equilibrium configuration and thus reflect the accuracy with which these structures are predicted by the available quantum-chemical codes. As expected, structures are easier to calculate than energies; hence the relative splittings are predicted more accurately than the absolute value of the zero-point splitting. The theory

also accounts for overtone and combination band splittings, provided anharmonic terms are small. Similarly, kinetic isotope effects are generally predicted with good accuracy, which again is an indication that the method accounts well for the transverse-mode contributions to the tunnelling. There is evidence that anharmonic couplings associated with large amplitude motions are important in some cases. They are not included in the present form of the dynamics, partly because they complicate the calculations and partly because the required anharmonicities are not available either quantum-chemically or spectroscopically. In the preceding section we have shown that it is possible to include such anharmonic couplings in the dynamics, but in the absence of calculated or observed anharmonicity parameters these couplings enter as adjustable parameters and are thus outside the scope of the present comparison of theory and experiment.

4.2. *Rate constants*

We now consider applications to tunnelling rate constants. To deal properly with their temperature dependence, we need an accurate representation of the shape of the potential, since upon approaching the cross-over temperature $T^* = \omega^*/2\pi k_B$, where ω^* is the imaginary frequency of the transition state, the tunnelling paths move close to the top of the barrier. Thus whereas for tunnelling splittings it is often sufficient to represent the potential accurately in the bottom region only, for rate constants an accurate description near the top is of equal importance. For symmetric barriers calculations at the stationary points yield the transfer distance, the barrier height (which may be in need of empirical adjustment), and the curvatures at the top and the bottom. However, there is no unique way to generate a potential from these four parameters. To model the potential accurately, the calculation of a few intermediate points will generally be advisable, especially for asymmetric potentials.

In this subsection we review four molecules, three of which undergo molecular inversion while the fourth undergoes tautomerization. The inversions differ from the hydrogen transfers considered above in that no bond is broken, but they show all the characteristics of a tunnelling reaction. In these systems, the tunnelling vibration is, however, a low-frequency mode, so that its coupling with high-frequency modes can be treated adiabatically through equation (28). Our earlier treatment of these three molecules [19] was incorrectly based on the normal coordinates of the equilibrium configuration rather than on those of the transition state. Here we report corrected results.

4.2.1. *Oxiranyl and aziridine*

First we review an early application of the theory to two simple triangular species, the aziridine molecule [19, 53–55] and the oxiranyl radical [19, 56], both illustrated in figure 4. The reported rate constants for molecular inversion show the characteristic kinetic isotope effect and temperature dependence of a hydrogen tunnelling process. They are measured by modelling the change of the magnetic resonance spectrum with temperature: at low temperatures these spectra reflect the non-planar equilibrium configuration and at high temperatures, the average over the two equilibrium configurations which corresponds to the planar transition state. At intermediate temperatures the gradual transition between the two spectra is used to evaluate the rate of inversion.

The stationary-state structures and force fields are calculated at the HF/6-31G** level and for oxiranyl also at the QCISD/6-311+G** level [19, 57]. The results ob-

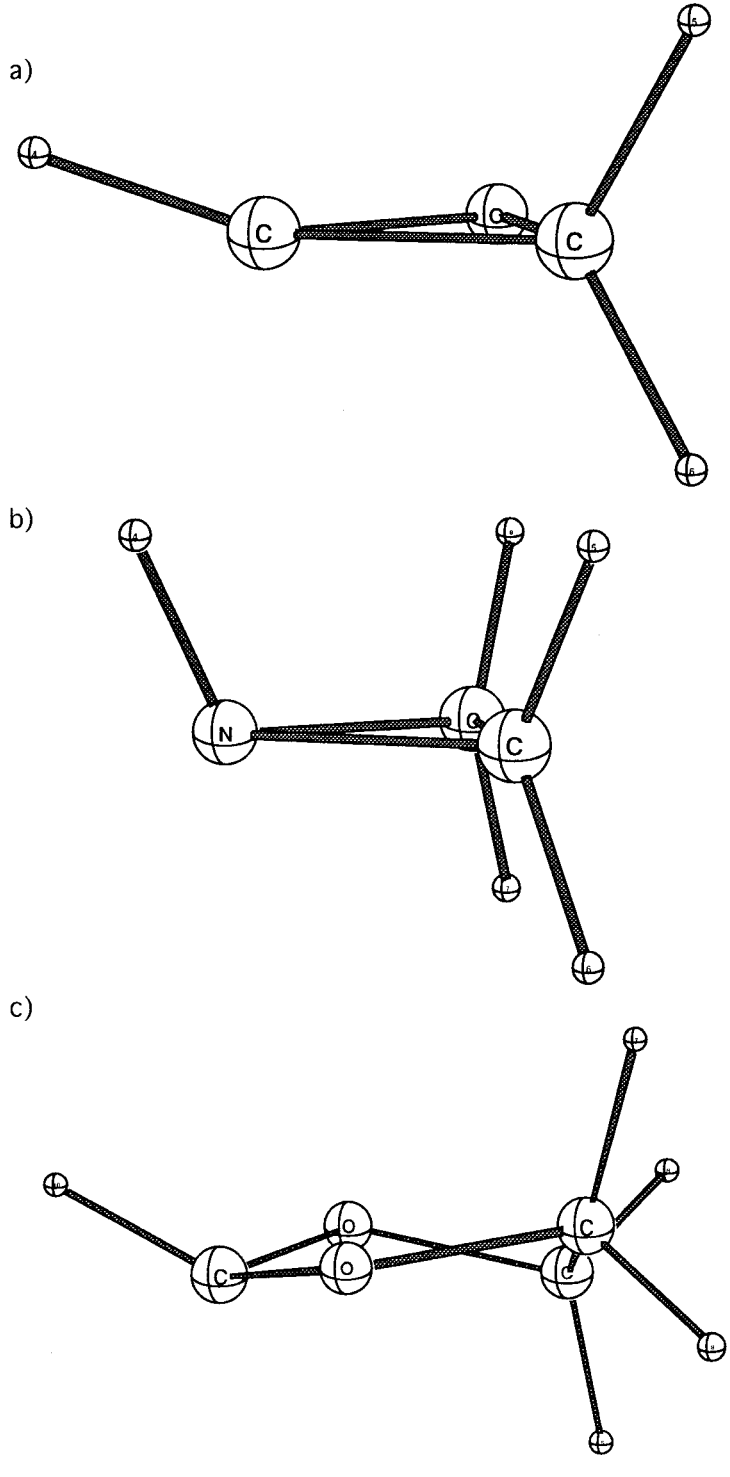

Figure 4. (*a*) Oxiranyl, (*b*) aziridine and (*c*) dioxolanyl.

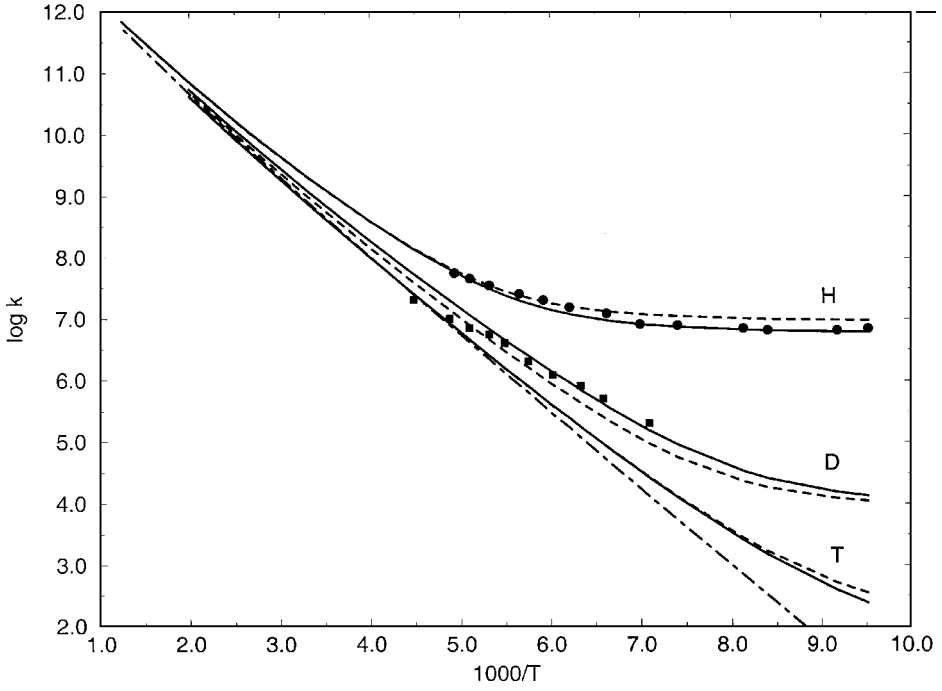

Figure 5. Comparison of calculated (solid lines) and observed (points) inversion rate constants of oxiranyl (top), oxiranyl-d_1 (centre), and oxiranyl-t_1 (bottom). The broken lines are obtained if the coupling to transverse modes is ignored. The dot-dash line is the classical over-the-barrier result for the light isotopomer.

tained at both levels are very similar if the HF frequencies are scaled by a factor of 0.9. For oxiranyl and its mono-deuterio and mono-tritio isotopomers, the imaginary frequencies at the top of the barrier are calculated to be 886i, 695i, and 618i cm^{-1}, respectively. These values extrapolate to Ω_0 values of 2080, 1452, and 1191 cm^{-1}, compared to equilibrium inversion frequencies of 803, 652, and 571 cm^{-1}, respectively. The adiabatic barrier height of 7.12 kcal mol^{-1} was scaled by a factor of 0.91 to 6.5 kcal mol^{-1}. This scaling serves to reproduce the temperature-independent rate constant of oxiranyl observed at low temperatures. The only mode significantly coupled to the inversion is the high-frequency CH(D)-stretching mode of the tunnelling proton (deuteron), which can be treated adiabatically. The barrier shape was determined by the calculation of points $U_a(x)$ for $0 < |x| < \Delta x$, all scaled by the same factor. Since in this case the potential is basically one-dimensional, the intermediate points could be calculated by projecting the minimum-energy path directly onto the reaction coordinate x. Figure 5 shows that the calculated inversion rate constants, including both classical and non-classical contributions, compare favourably with experiment. The dot-dash line, which represents the classical contribution for the light isotopomer, shows that tunnelling transfer dominates below 350 K. For the D and T isotopomers, the corresponding temperatures are 300 K and 225 K, respectively. The broken lines show the results obtained without coupling to the high-frequency stretching mode; in the present case the coupling is very weak and produces only a small correction.

The results for aziridine are somewhat different in that there is coupling to

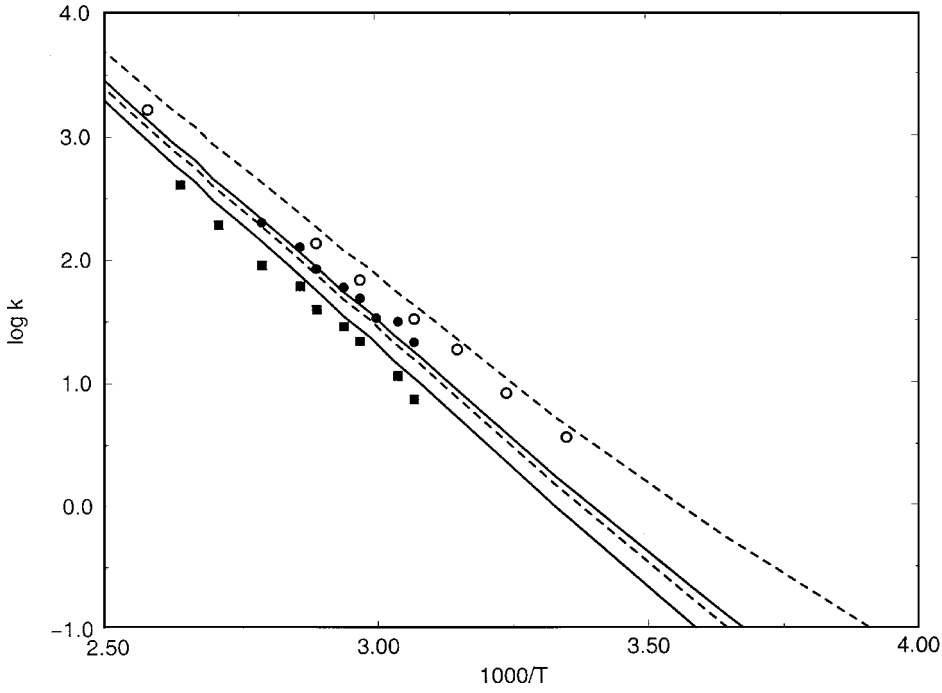

Figure 6. Comparison of calculated (solid lines) and observed (points) inversion rate constants for aziridine (top) and aziridine-d_1 (bottom). Open and closed symbols refer to data of [53] and [54], respectively. The broken lines represent results if the coupling is ignored.

low-frequency antisymmetric modes, which has a suppressing effect on the inversion. The kinetic experiments were carried out at much higher temperatures than for oxiranyl and show a good deal of scatter [53, 54], as illustrated in figure 6. The calculated results are very close to the classical limits in the range of temperatures where kinetic data are available.

4.2.2. *Dioxolanyl*

The dioxolanyl radical, illustrated in figure 4, also shows inversion by tunnelling [19, 58], but in this case the rate of inversion has been measured only for the mono-deuterio compound, the rate in the undeuterated radical being too fast to be observed by EPR spectroscopy. Relative to the earlier treatment [19], the level of the calculation has been upgraded to DFT/UB3LYP/6-31G* [57], a method which, for inversions, was found to be equal or superior to MP2 or QCISD methods with larger basis sets. It is found that the inversion mode of 720 cm^{-1} in the transition state couples strongly with two symmetric transverse modes, a high-frequency mode of 2496 cm^{-1}, which is included via mass renormalization through equation (28), and a low-frequency mode of 247 cm^{-1}, which corrects the instanton action through equations (20) and (22). The barrier height was calculated to be 2064 cm^{-1} and the barrier shape was approximated by the quartic potential (14). After scaling the barrier by a factor 0.99, we obtained the calculated rate constants shown in figure 7, where they are compared with experiment. We also list results for the undeuterated

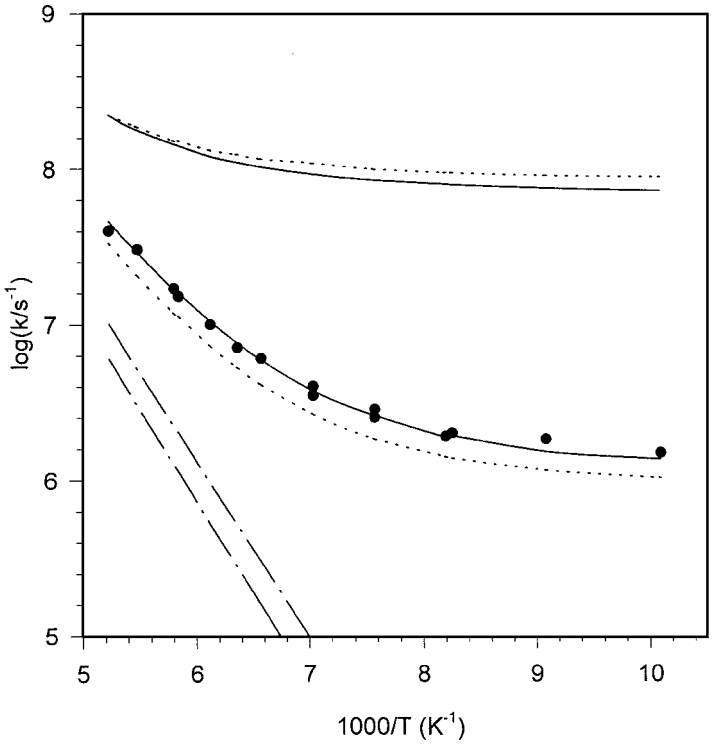

Figure 7. Comparison of calculated (solid lines) and observed (points) rate constants for dioxolanyl (top) and dioxolanyl-d_1 (bottom). The dotted lines are obtained if coupling to transverse modes is ignored. The dot-dash lines represent classical results.

compound to show that these are indeed predicted to be outside the range accessible by magnetic resonance spectroscopy.

4.2.3. *Porphyrins*

To conclude our comparison with experiment we consider double-hydrogen transfer in porphine, depicted in figure 8. This is a much studied molecule for which excellent kinetic data are available, covering a wide range of temperatures [59–61]. Two-proton transfer can occur by two mechanisms: coherently, when the protons move in phase, and incoherently, through a *cis*-type intermediate, as illustrated in figure 8. It has been recognized for some time [14, 59, 62–65] that the latter process dominates for all temperatures for which data are available. This means that the transfer rate is controlled by transfer of a single proton across an asymmetric barrier between the stable *trans* and the metastable *cis* compound. Direct evidence for this conclusion can be derived from low-temperature rate constants [59], which show the same temperature dependence for hydrogen as for deuterium transfer, from which the *cis–trans* energy difference can be directly estimated, since it indicates that the low-temperature limit has been reached where tunnelling transfer occurs exclusively at the zero-point level of the *cis* isomer and hence is independent of temperature.

A simpler version of the same problem is obtained if one of the protons is removed to create the porphine anion. Also kinetic data are available for this anion [66], but in a more restricted range of temperatures than for porphine itself. In the

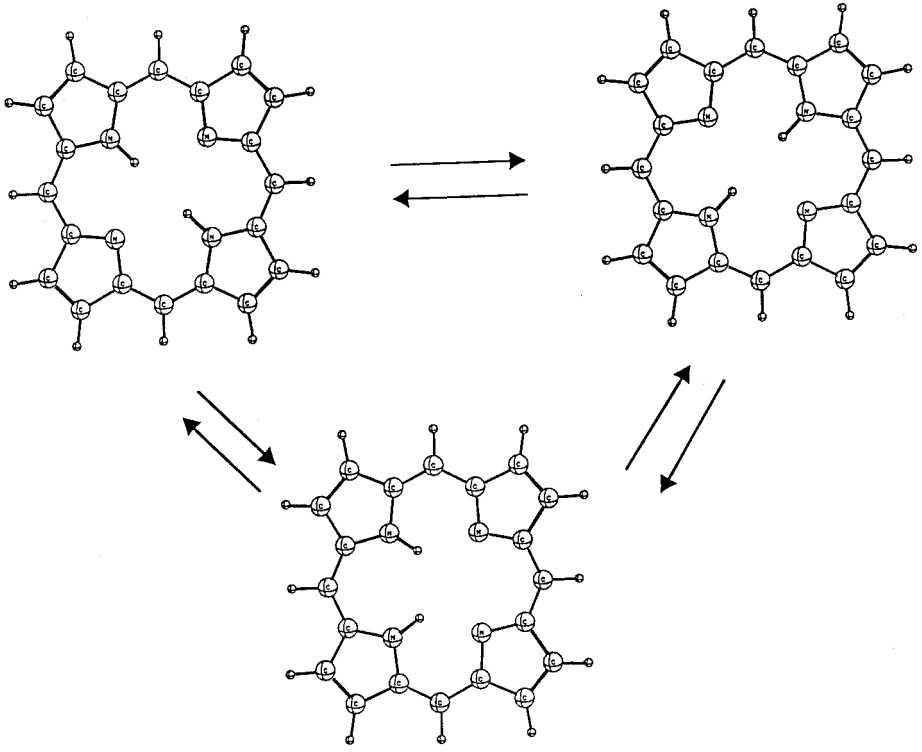

Figure 8. The two reaction pathways for tautomerization of porphine.

anion the barrier is symmetric so that at low temperatures the rate constant should go to a non-zero limit. Whereas in porphine tunnelling can occur only at energies above the energy of the *cis* isomer, in the anion there are no energy restrictions, and hence the transfer will be faster, especially at lower temperatures. An analysis of the anion data by our method is in preparation and will be published elsewhere.

It has been found that density-functional theory at the B3LYP/ 6-31G* level gives an accurate account of the structure and force field of porphine in its equilibrium configuration [67, 68]. Therefore this is the method we have used to evaluate the transfer potential. It should be realized, however, that this method need not be equally successful for the transition state in which there are hydrogen bonds, whose strength is likely to be overestimated by density-functional theory, leading to low barriers and possibly short tunnelling distances. Unfortunately, calculations at the alternative Hartree–Fock level produce unacceptable structures. Therefore we have limited such calculations to the DFT-optimized stationary structures.

From the low-temperature kinetic data [59] the *cis–trans* energy difference is estimated to be $2200 \pm 300\,\mathrm{cm}^{-1}$; the values obtained by the DFT and HF methods are 2900 and $3900\,\mathrm{cm}^{-1}$, respectively, which indicates that neither method yields accurate energies. This holds true *a fortiori* for the adiabatic barrier height for which the two methods give 5850 and $8600\,\mathrm{cm}^{-1}$, respectively [26].

The problem of the shape of the barrier has been approached in several ways. The simple analytical potentials discussed in section 2.3 were found to be unsatisfactory. A simplified way to calculate intermediate points has been discussed before [26];

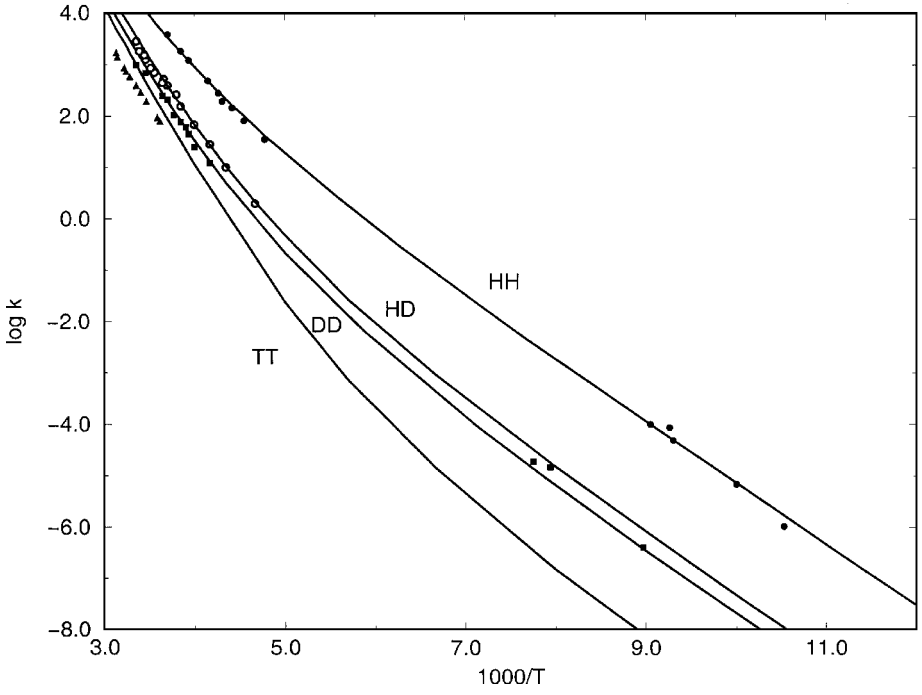

Figure 9. Comparison of calculated (solid lines) and observed (points) tautomerization rate constants of four isotopomers of porphine.

starting from points along the minimum-energy path, it assumes that distances along this path are proportional to distances along the reaction coordinate x. This works reasonably well for porphine, as shown before [26]. As an alternative, we report here results based on a potential that reflects all six stationary-point parameters with the respective points and curvatures connected by smooth interpolation, the connecting lines being drawn as tangents to the calculated curves.

The calculated rate constants for the tautomerization reaction in porphine obtained with this potential are compared with experiment in figure 9. The overall agreement is seen to be satisfactory considering the wide range of temperatures and isotopic masses, resulting in rate constants spanning 10 orders of magnitude. The observed transfer rates are all in the tunnelling region. The temperature where the classical and non-classical contributions to the rate in porphine are equal varies from about 450 K for the TT isotopomer to more than 700 K for the HH compound, showing that tunnelling is the transfer mechanism for all temperatures of practical interest. The calculations underestimate the isotope effect, which is particularly evident in the case of the TT isotopomer. It is possible to correct this by changing the shape of the barrier [26], specifically by slimming down the upper part, but for the moment we are not aware of a theoretical justification for such a procedure.

4.2.4. *Summary of rate constants*

Summarizing the results of this subsection, we conclude that the present procedure is as successful for rate constants as it was shown to be for splittings. In

particular, the method proved to be capable of dealing with transfer through an asymmetric barrier in a molecule as large as porphine. In addition to handling actual proton transfer, the theory also applies to low-frequency tunnellings such as molecular inversions and covers the entire range of temperatures from low-temperature tunnelling to high-temperature classical transfer. The present level of dynamics seems sufficient for practical purposes, since uncertainties in the quantum-chemically computed parameters tend to be much larger than the uncertainties introduced by the present instanton approach. The main problem is the uncertainty of the calculated barrier height; this of course affects all dynamics methods.

The method is not limited to temperature-averaged rate constants but can also be applied to rate constants for a specific vibronic level. The procedure is similar to that described in the preceding sections for mode-specific splittings.

5. Other applications

Applications to molecules for which no experimental rate constants or splittings are available amount to predictions. In view of the uncertainties in the available potentials, the predicted absolute values will rarely turn out to be accurate. However, such predictions may shed light on relative rates and splittings as well as on transfer mechanisms.

5.1. *Malonaldehyde*

Proton transfer in malonaldehyde, depicted in figure 1, has served as a prototype for transfer in hydrogen-bonded systems [43–51]. There have been several attempts to calculate the zero-point splitting in the ground state [9, 21, 44–49, 69] but the uncertainty in the calculated barrier heights prevents usage of these results as a test for the dynamics used in these calculations. Although no mode-specific tunnelling splittings have been measured for malonaldehyde, we have calculated these splittings in response to calculated splittings in the literature [9], which did not show the expected dependence of the splitting on the symmetry of the excited modes. Our own, so far unreported, calculations show the expected behaviour, which suggests that the older estimates are incorrect.

These calculations for mode-specific splittings in the ground state follow the same routine as reported for 9HPO and produce similar results. At the HF/6-31G** level, an adiabatic barrier height of 10.3 kcal mol^{-1} (3590 cm^{-1}) was obtained. At this level the calculated structure in the hydrogen-bonded region deviates appreciably from the structure deduced from microwave spectroscopy. The observed zero-point splittings of 21.6/3.0 cm^{-1} for H/D transfer are reproduced if the barrier is scaled by a factor 0.95. In that case our calculation predicts enhanced splittings for symmetric CCC-deformation modes, namely 99 and 42 cm^{-1} for modes with calculated (observed) frequencies of 248 (252) and 866 (873) cm^{-1}, and a reduced splitting of 17 cm^{-1} for the antisymmetric CCO-deformation mode at 480 (511) cm^{-1}.

To obtain more reliable predictions, it will be necessary to upgrade the quantum-chemical calculations to the point where they are capable of reproducing the observed structure and barrier height. Such calculations have been performed and are now being extended to the transition state [70].

5.2. *Complexes with solvent molecules*

Tunnelling calculations may help us understand the catalytic activity of solvent molecules such as water in hydrogen transfer processes. The ionization of weak

acids is such a process, where the relative rates of hydrogen transfer and solvent reorganization have been probed experimentally and theoretically, e.g. in the case of excited phenol- and naphthol-ammonia complexes [71–76].

In these systems proton transfer from phenol (naphthol) to a hydrogen-bonded ammonia molecule occurs upon excitation of the aromatic component, provided the complex contains at least five (three) ammonias. The transfer can be monitored by fluorescence and by multiphoton ionization and typically cannot be characterized by a single first-order rate constant. The experimental results were originally interpreted as indicative of a biexponential process, namely proton transfer followed by solvent reorganization. However, this interpretation left many observations unexplained and disagreed with the results of our theoretical model study [75]. Our calculations on excited phenol-$(NH_3)_5$ indicate that the solvent reorganization associated with the proton transfer is a simple barrierless process along a single low-frequency normal coordinate of the complex with a time constant of the order of a picosecond. Since the smaller of the two time constants $1/k$ derived from the transfer data is about 50 ps, this means that neither this nor the larger time constant of about 350 ps can be associated with solvent reorganization, in keeping with the observation that in the corresponding naphthol complex both rate constants are subject to strong deuterium effects.

To firm up these conclusions we have extended our original one-dimensional tunnelling calculations on the phenol complex [75] to full multidimensional calculations for single vibronic levels, using the method discussed in this review. The results lead to mode-specific rate constants in the region covered by the excitation wavelength, the lowest of which, corresponding to the zero-point level, amounts to $2 \times 10^9\ s^{-1}$ ($2 \times 10^8\ s^{-1}$ for deuterium transfer), comparable to the observed larger time constant of 350 ps for the undeuterated molecule. There are several antisymmetric modes coupled to the tunnelling mode and their excitation would tend to increase the rate of transfer by reducing the corresponding Franck–Condon effect, thereby decreasing the time constant towards the smaller observed value [76]. However, it is not clear to what extent these modes are excited in the experiment, so that a detailed explanation of the observed kinetics cannot be given at this time.

Another example is the transfer of a proton between the two tautomers of 7-azaindole catalysed by a complexed water molecule [77]. In this complex, illustrated in figure 10, the water molecule forms hydrogen bonds with the donor and acceptor nitrogen atoms, leading to synchronous transfer of two hydrogens. The adiabatic barrier height relative to the energy of the metastable tautomer, calculated at the HF/6-31G* level, was found to be $26.7\ kcal\,mol^{-1} = 9325\ cm^{-1}$, a value slightly higher than the result of Gordon [77]; both values are likely to be too high by several $kcal\,mol^{-1}$. The transfer, which is exothermic by $13.1\ kcal\,mol^{-1} = 4580\ cm^{-1}$, is greatly accelerated by coupling of the tunnelling mode to several symmetric modes, so that, for example, at room temperature, the rate constant is 3–4 orders of magnitude higher than that of the one-dimensional process. The classical contribution to the rate is completely negligible at all temperatures of practical interest for both isotopomers. In figure 11 we report preliminary results for the double-hydrogen transfer rate constants with and without deuteration of the mobile hydrogen atoms. These results, which predict a lifetime of a few milliseconds for the metastable isomer in water, show the strong catalytic effect of water, which greatly accelerates the process, as illustrated in figure 11, where the dashed line represents the rate constant of single-proton transfer in isolated 7-azaindole.

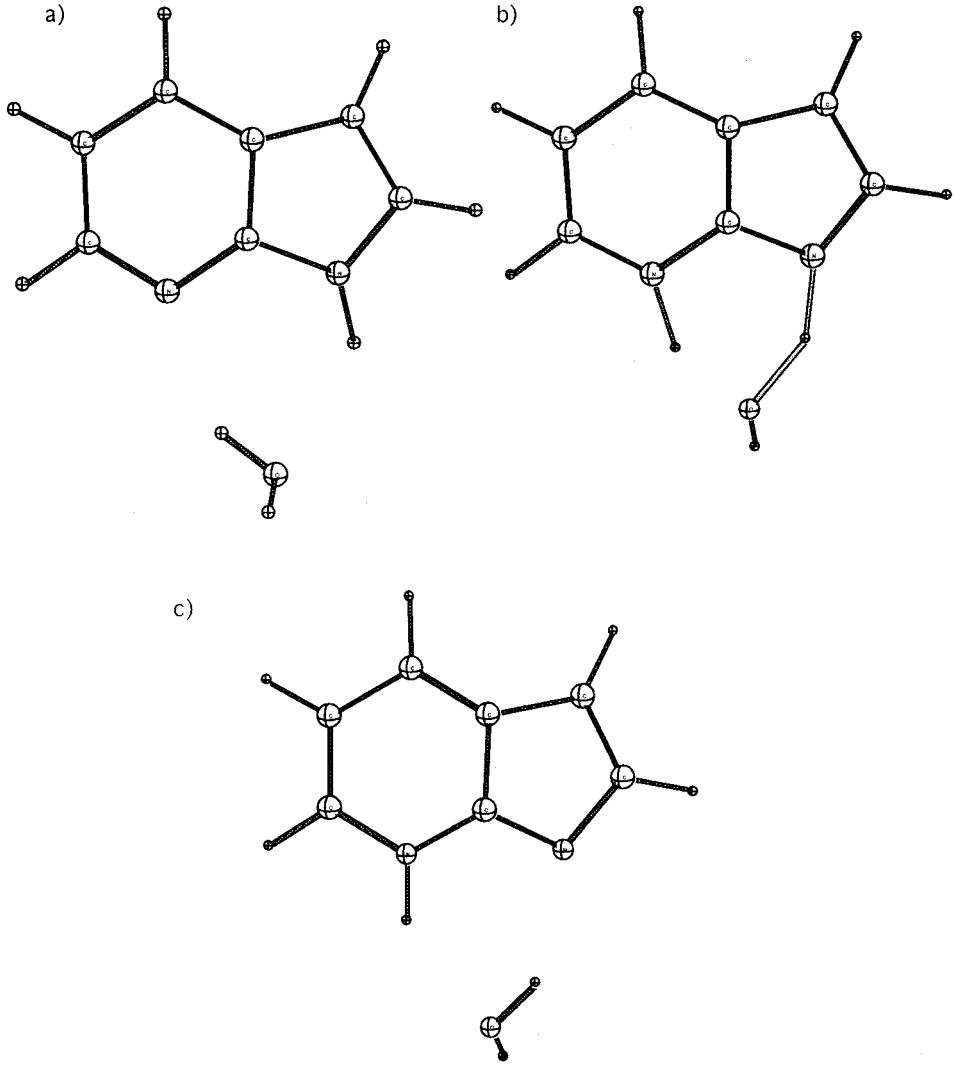

Figure 10. 7-Azaindole·H_2O; the structures (*a*) and (*c*) represent the stable and metastable isomer, respectively, and (*b*) represents the transition state between them.

5.3. *Anharmonic couplings*

The applications described in the preceding section are based on *ab initio* calculations without free parameters. Specifically they invoke the simplifying assumptions that the transverse modes are harmonic and linearly coupled to the tunnelling mode. This assumption, which implies the absence of anharmonic terms in the transverse-mode potential, is difficult to avoid in an *ab initio* context, since the available quantum-chemical codes have great difficulty in dealing with such anharmonicity. As a result the dynamics cannot be readily extended to anharmonic potentials unless freely adjustable anharmonic coupling parameters are introduced, implying a departure from the *ab initio* protocol.

The presence of non-negligible anharmonic couplings between the tunnelling

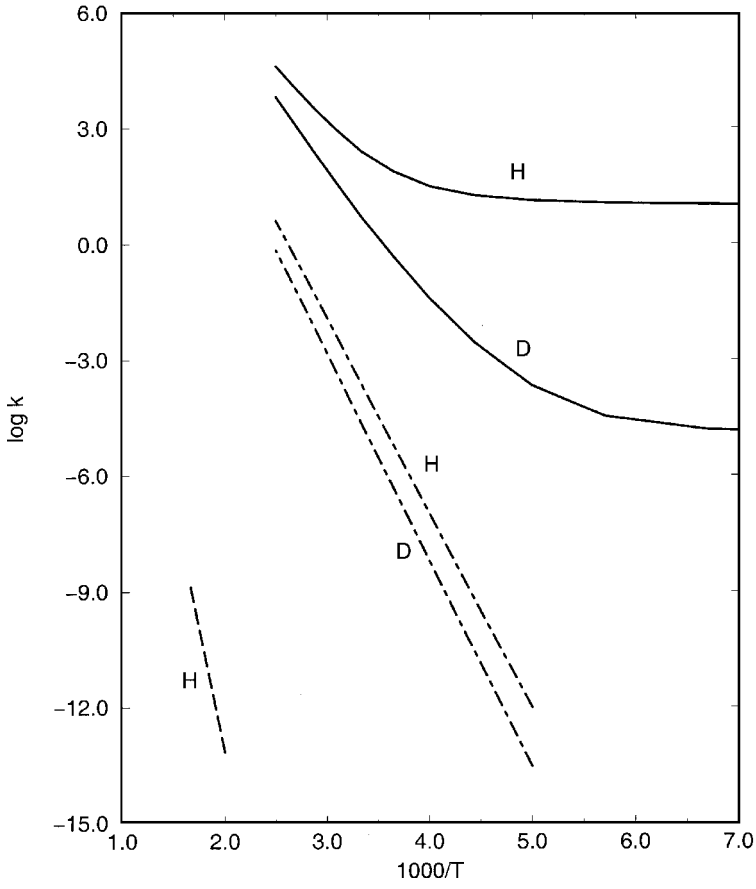

Figure 11. Calculated double-hydrogen transfer rate constants in 7-azaindole·H_2O (solid lines) and the corresponding classical approximation (dot-dash lines). The dashed line refers to transfer in bare azaindole.

mode and large-amplitude transverse modes can be deduced directly from experiment. A typical example, mentioned in the preceding section, is tropolone [22, 41] in which the tunnelling splitting in the fluorescent state is observed to decrease progessively with the level of excitation of low-frequency out-of-plane modes. Since the molecule remains planar during proton transfer, these modes are not displaced and thus not linearly coupled to the tunnelling mode. The lowest-order coupling compatible with the symmetry of the molecule is biquadratic in the two coordinates. A similar observation has been made for indoline [20] where the ring-puckering vibration is the tunnelling mode; in this molecule the tunnelling splitting is observed to increase progressively with increasing excitation of the low-frequency butterfly mode, which is not displaced by the transfer. Anharmonic couplings have also been invoked to explain tunnelling splittings in methylglycolate [24].

We now show that these problems can be handled by the formalism developed at the end of section 3. In a few cases the required anharmonic couplings, chosen so as to fit an appropriate set of experimental data, have been compared with calculated values. To minimize arbitrariness, we only discuss cases where a single coupling constant can interpret multiple observations. This is the case in tropolone where the

lowest-frequency mode, $\omega_{26} = 37.5\,\mathrm{cm}^{-1}$, shows a progression $v = (0), 2, 4, 6, 8, \ldots$, in the fluorescence-excitation spectrum for which the splitting decreases from $18.9\,\mathrm{cm}^{-1}$ to 7.2, 4.7, 3.5, and $0.8\,\mathrm{cm}^{-1}$, respectively [41]. From equation (35) we obtain 10, 5.1, 2.3, and $0.8\,\mathrm{cm}^{-1}$, repectively, if we assume an anharmonic coupling constant $D_{26} = -26\,\mathrm{cm}^{-1}$, a value considerably smaller than the theoretically estimated value of $-39\,\mathrm{cm}^{-1}$ [22].

In indoline, on the other hand, the calculated anharmonic coupling between the tunnelling mode and the butterfly mode is positive, leading to the prediction of an increase in the splitting with increasing excitation of the latter mode. This is indeed observed: in the progression $v = (0), 1, 2, \ldots$, the splitting increases from (14.6) to 570 and $9000\,\mathrm{cm}^{-1}$, in good agreement with the calculated values of (14.8), 530, and 11000 cm^{-1} obtained with the calculated anharmonic coupling parameter of $21\,\mathrm{cm}^{-1}$ [20].

6. Conclusions

The main conclusion we wish to draw from this work is that for typical hydrogen transfer processes whereby an XH bond is broken and a new HY bond is formed, the transfer is dominated by tunnelling at most temperatures of practical interest, including room temperature. If this fact is ignored, calculated transfer rate constants may be too small by orders of magnitude. For deuterium transfer the cross-over to classical transfer occurs at lower temperatures but usually well above room temperature. Thus the observation of an apparently linear Arrhenius plot for hydrogen or deuterium transfer over a narrow range of temperatures does NOT justify the conclusion that the transfer is classical; the corresponding Arrhenius slope can thus not be used to obtain the barrier height.

Deuterium and tritium isotope effects are widely used in organic chemistry and biochemistry to analyse the mechanism of complex reactions. Unfortunately, the theory used to interpret these results is often of dubious validity. One of the purposes of the present review is to demonstrate that simple one-dimensional tunnelling models do not provide a reliable basis for such interpretations. At the same time we offer a method which makes it possible to deal efficiently with large systems without invoking untenable approximations. Benchmark comparisons indicate that of the methods available to date, the instanton method discussed here is clearly the most accurate and most efficient; specifically, it was found to be about three orders of magnitude faster than methods based on variational transition-state theory with semiclassical tunnelling corrections. Contrary to the latter theories, it can provide mode-specific tunnelling splittings and temperature dependent rate constants down to $T = 0\,\mathrm{K}$ for almost any system that can be handled by the available quantum-chemical codes. While routine estimates of rate constants and splittings can be readily obtained through the use of our DOIT code [27], the strong dependence of the results on the calculated barrier heights indicates that a judicious choice among the available quantum-chemical methods is essential if accurate values are to be obtained.

The method is designed to deal with multidimensional systems and has been tested on medium and large molecules, ions and radicals in the gas phase and in solution. In addition preliminary results have been obtained on complexes with solvent molecules where the tunnelling involves proton transfer between solute and solvent. Of particular interest are complexes in which solvent molecules such as water catalyse intramolecular proton transfer, since such processes are likely to be

important in biological systems. Testing of the method on such systems is hampered by the lack of experimental data. That tunnelling is likely to be important in higher organisms follows from the fact that heavy water is toxic. On the other hand, bacteria can be deuterium-labelled by immersion in heavy water. Although substantial deuterium isotope effects have been reported for a number of enzymatic reactions, it is difficult to interpret these results unambiguously. An important first step towards such an analysis, would be the integration of the instanton method in a quantum-simulation protocol, a project that will be the subject of a future report.

Appendix

In this Appendix we provide some mathematical background to the instanton model. The observation of a first-order rate constant implies that the levels monitored have a Lorentzian linewidth, which is proportional to the tunnelling probability and can be represented by an imaginary term $\Gamma(E) = 2\,\mathrm{Im}\,E$ in units $\hbar = 1$. We first consider transfer in a one-dimensional double-well potential $U(x)$ with a barrier height U_0 at $x = 0$ and a frequency ω_0 at the bottom of the wells. The transfer rate constant is the Boltzmann average over the initial states and can be approximated quasiclassically by

$$k = Z_0^{-1} \int_0^\infty \mathrm{d}E\, \rho(E)\Gamma(E)\, \exp(-\beta E), \tag{A 1}$$

where $\beta = 1/k_B T$, $\rho(E)$ is the density of final states, and

$$Z_0 = \sum_{n=0}^{\infty} \exp(-E_n\beta) \simeq (2\,\sinh\,\omega_0\beta/2)^{-1} \tag{A 2}$$

is the partition function. For $E < U_0$ the tunnelling probability is given by [36]

$$\rho(E)\Gamma(E) = \exp\left\{-2\int_{x_1}^{x_2} \mathrm{d}x\,[2(U-E)]^{1/2}\right\} = \exp[-2S(E)], \tag{A 3}$$

where $x_{1,2}$ are classical turning points for energy E and $S(E)$ is the classical action. For $E \geqslant U_0$ the top part of the barrier can be represented by an inverted parabola which leads to [78]

$$\rho(E)\Gamma(E) = \frac{1}{1 + \exp[-2\pi(E-U_0)/\omega^*]}, \tag{A 4}$$

where $\mathrm{i}\omega^*$ is the imaginary frequency at the top. This expression goes to unity for high energies and connects smoothly to equation (A 3) in the tunnelling region.

In the integral of equation (A 1) the energy-dependent factor $\rho(E)\Gamma(E)$ competes with the Boltzmann factor. In the tunnelling region, we have from equations (A 1) and (A 3)

$$-2\frac{\partial S(E)}{\partial E} = \beta, \tag{A 5}$$

which determines the energy E^*, where $S(E)$ reaches its minimum value. Alternatively we have

$$\frac{\partial S(E)}{\partial E} = -\int_{x_1}^{x_2} \frac{\mathrm{d}x}{[2(U-E)]^{1/2}} = -\tfrac{1}{2}\Theta(E), \tag{A 6}$$

where $\Theta(E)$ is the period of the motion of the tunnelling particle in the upside-down potential $-U$. Combining these results, we find that $\beta = \Theta(E^*)$ defines the

energy value that dominates the integral (A 1). Evaluation of (A 1) by the method of steepest descent yields

$$k = \frac{\exp(-2S_E - \beta E^*)}{Z_0\{2\pi[\partial\Theta(E)/\partial E]_{E^*}\}^{1/2}}, \tag{A 7}$$

where S_E is the Euclidian action

$$S_E = \int_0^\beta d\tau\, H[x(\tau)], \tag{A 8}$$

with the Hamiltonian $H = \dot{x}^2/2 + U$ replacing the usual Lagrangian since the integration is over imaginary time $\tau = it$. Since $\Theta(E^*) \geqslant 2\pi/\omega^*$, the corresponding extremal tunnelling trajectory applies only below the cross-over temperature $T^* = 2\pi/\omega^* k_B$.

To generalize this approach to multidimensional systems, we rewrite equation (A 1) as a sum over states

$$k = \mathrm{Re}\, Z^{-1} \sum_n \exp(-\beta\, \mathrm{Re}\, E_n)\, \mathrm{Im}\, E_n, \tag{A 9}$$

which can be rewritten in the form [35]

$$k = 2\beta^{-1}\, \mathrm{Im}\, Z/\mathrm{Re}\, Z. \tag{A 10}$$

The advantage of this formulation is that the partition function can be expressed in terms of integrals over all possible paths, each path modulated by an appropriate phase factor. The resulting path integral allows straightforward generalization to multidimensional transfer.

To show this, we start from the evolution operator that expresses the amplitude at time t of a particle moving in a one-dimensional potential $U(x)$ and express it as a path integral

$$K(x, x_0, t) = \langle x(t)|\, \exp(-iHt)|x(0)\rangle = \int D[x(t)]\, \exp(iS[x(t)]), \tag{A 11}$$

where S is the classical action along a specified path

$$S[x(t)] = \int_0^t dt'\, L(x, \dot{x}), \tag{A 12}$$

$L = \frac{1}{2}\dot{x}^2 - U(x)$ being the Lagrangian. To proceed, it proves convenient to change variables. We note that expansion of the evolution operator in terms of the eigenfunctions ϕ_m of H, namely,

$$K(x, x_0, t) = \sum_m \phi_m[x(t)]\phi_m^*[x(0)]\, \exp(-iE_m t), \tag{A 13}$$

leads to a form equivalent to the density matrix

$$\rho(x, x') = \sum_m \phi_m(x')\phi_m(x)\, \exp(-\beta E_m) \tag{A 14}$$

if we make the substitution $it \rightarrow \beta$. The transformation $t \rightarrow -i\tau$, $x \rightarrow x$, $\dot{x} \rightarrow -i\dot{x}$, $U(x) \rightarrow -U(x)$, and $E \rightarrow -E$ formally turns the barrier upside down. The result is that the density matrix can now be written as a path integral for the

Euclidian action

$$\rho[x(\tau), x(0)] = \int_{x(0)}^{x(\tau)} D[x(\tau)] \exp\{-S_E[x(\tau)]\}, \tag{A 15}$$

$$S_E[x(\tau)] = \int_0^\beta d\tau\, H[x(\tau), \dot{x}(\tau)]. \tag{A 16}$$

This means that the partition function

$$Z = \mathrm{Tr}\,\rho = \int dx\, \rho(x, x) \tag{A 17}$$

can be expressed as a path integral over closed trajectories $x(\tau) = x(0)$:

$$Z = \int dx(0) \int_{x(0)=x(\tau)} D[x(\tau')] \exp\{-S_E[x(\tau')]\}. \tag{A 18}$$

This equation can be directly generalized to an arbitrary number of degrees of freedom. For our set of vibrational coordinates $x, \mathbf{y}$ the result is

$$Z = \int dx(0)\, d\mathbf{y}(0) \int_c D[x(\tau)] D[\mathbf{y}(\tau)] \exp\{-S_E[x(\tau), \mathbf{y}(\tau)]\}, \tag{A 19}$$

where the second integration is over closed paths $x(\tau) = x(0)$, $\mathbf{y}(\tau) = \mathbf{y}(0)$.

For the multidimensional system (A 19), the instanton trajectory can be calculated by solution of a set of $n + 1$ classical equations of motions, if n is the number of coupled transverse modes. Since this is generally impractical except for the smallest systems, one normally introduces approximations at this point. For instance one can lump all transverse modes together and use y as an effective-mode coordinate or one can treat these modes collectively as a heatbath. However, neither of these approaches is satisfactory for molecules, where the coupled modes span a wide range of frequencies and where their effect can help or hinder tunnelling depending on their symmetry. To obtain a more appropriate simplification, we start with the assumption that all transverse modes are harmonic and are linearly coupled to the tunnelling mode. For a particular mode y with a coupling constant C this leads to a classical equation of motion for a forced harmonic oscillator:

$$\ddot{y} = -Cf(x) - \omega^2 y, \tag{A 20}$$

where $f(x)$ is an arbitrary function of x which in our case equals x or x^2.

This forced-oscillator equation can be solved analytically for appropriate periodic boundary conditions:

$$\begin{aligned} y(\tau) = {} & \frac{\chi(\beta - \tau)}{\chi(\beta)} y(0) + \frac{\chi(\tau)}{\chi(\beta)} \{y(\beta) \\ & + C \int_0^\beta d\beta' f[x(\beta')] \chi(\beta - \beta')\} \\ & - C \int_0^\tau d\beta' f[x(\beta')] \chi(\tau - \beta'), \end{aligned} \tag{A 21}$$

where $\chi(z) = [\sinh(\omega z)]/\omega$. The additive contribution of this oscillator to the Euclidian action can be obtained by substitution of the result into an equation of

the form (A 7):

$$\delta S_{\mathrm{E}} = \int_{-\beta/2}^{\beta/2} \mathrm{d}\tau \{\dot{y}^2/2 + \omega^2 y^2/2 + Cf[x(\tau)]y\}. \tag{A 22}$$

The resulting Gaussian integrals can be evaluated analytically. This eliminates the explicit dependence on the transverse coordinates, so that the problem becomes effectively one-dimensional with time-retarded interactions expressing the memory effect of the coupled transverse modes on the proton transfer. The time-retarded potential is represented by the kernel $\Xi(\tau - \tau')$ in the expression

$$S_{\mathrm{E}}[x(\tau)] = \int_{-\beta/2}^{\beta/2} \mathrm{d}\tau \{\dot{x}^2/2 + U_a(x) + C^2/4\omega^3 \times \int_{-\tau}^{\tau} \mathrm{d}\tau' \frac{\mathrm{d}f[x(\tau)]}{\mathrm{d}x} \frac{\mathrm{d}f[x(\tau')]}{\mathrm{d}x} \dot{x}(\tau)\dot{x}(\tau')\Xi(\tau - \tau')\}, \tag{A 23}$$

where

$$U_{\mathrm{V,ad}} = U(x) + \tfrac{1}{2}[\omega - C^2\omega^{-2}f(x)^2] \tag{A 24}$$

is the vibrationally-adiabatic potential. For the complete expression of the kernel, we refer to the original literature [17, 18] . In practice it is often sufficient to consider limiting cases. For high-frequency transverse modes or low temperatures, only zero-point motions contribute. Then the kernel simplifies to

$$\Xi(\tau - \tau') = \exp(-\omega|\tau - \tau'|). \tag{A 25}$$

For low-frequency transverse modes ($\omega \ll \Omega_0$) that are thermally activated, the kernel will be temperature-dependent but effectively independent of $\tau - \tau'$:

$$\Xi(\tau - \tau') = \coth(\beta\omega/2). \tag{A 26}$$

By definition, the instanton trajectory minimizes S_{E} and thus satisfies the Euler–Lagrange equation

$$-\ddot{x}(\tau) + \partial U_{\mathrm{V,ad}}/\partial x + (C^2/\omega^2) \int_{-\beta/2}^{\beta/2} \mathrm{d}\tau' \Xi(\tau - \tau')x(\tau') = 0, \tag{A 27}$$

where $x(\tau)$ is a periodic function $x(\tau) = x(\tau + \beta)$. So far the instanton trajectory has been found explicitly only for a few model one-dimensional potentials and within limited temperature ranges depending on the parameters involved. In the simple case where the symmetric double-well potential formed by two intersecting parabolas is coupled linearly to a totally symmetric transverse normal coordinate

$$U(x, y_s) = \tfrac{1}{2}\omega_0^2(|x| - \Delta x)^2 - C_s(|x| - \Delta x)y_s + \tfrac{1}{2}\omega_s^2 y_s^2, \tag{A 28}$$

the resulting 2×2 matrix can be diagonalized by rotating the coordinates over an angle ϕ such that [38]

$$\begin{aligned} \tan^2\phi &= \frac{\omega_+^2 - \omega_0^2}{\omega_0^2 - \omega_-^2}, \\ \omega_\pm^2 &= \tfrac{1}{2}\omega_0^2\{(\sigma^2 - 1) \pm [(\sigma^2 - 1)^2 + \gamma^2]^{1/2}\} \\ \sigma &= \omega_s/\omega_0, \\ \gamma &= 2C/\omega_0^2. \end{aligned} \tag{A 29}$$

This leads to the instanton action

$$S_I = 2\Delta x^2/[\omega_+^{-1}\cos^2\phi\coth(\beta\omega_+/4) + \omega_-^{-1}\sin^2\phi\coth(\beta\omega_-/4)]. \quad \text{(A 30)}$$

For a relatively weak coupling and low transverse-mode frequency, the sine and cosine functions can be simplified, leading to

$$S_I \simeq 2\Delta x^2/[\omega_0^{-1}\coth(\beta\omega_+/4) + (\gamma^2/\omega_s)\coth(\beta\omega_-/4)] \quad \text{(A 31)}$$

$$\simeq S_I^0/[1 + \tfrac{1}{4}\gamma^2(\omega_0/\omega_s)\coth(\beta\omega_s/4)],$$

$$S_I^0 = 2\Delta x^2\omega_0\tanh(\beta\omega_0/4) \quad \text{(A 32)}$$

being the action in the one-dimensional potential, which leads to equation (22).

Acknowledgment

The paper is issued as NRCC No. 40899.

References

[1] Truhlar, D. G., Garrett, B. C., and Klippenstein, S. J., 1996, *J. phys. Chem.*, **100,** 12771.
[2] Truhlar, D. G., Isaacson, A. D., and Garrett, B. C., 1985, *Theory of Chemical Reaction Dynamics*, Vol. 4, edited by M. Baer (Boca Raton: CRC Press).
[3] Garrett, B. C., and Truhlar, D. G., 1983, *J. chem. Phys.*, **79,** 4931.
[4] Miller, W. H., Handy, N. C., and Adams, J. E., 1980, *J. chem. Phys.*, **72,** 99.
[5] Skodje, R. T., Truhlar, D. G., and Garrett, B. C., 1981, *J. phys. Chem.*, **85,** 3019.
[6] Garrett, B. C., Joseph, T., Truong, T. N., and Truhlar, D. G., 1989, *Chem. Phys.*, **136,** 271.
[7] Waite, B. A., and Miller, W. H., 1980, *J. chem. Phys.*, **73,** 3713.
[8] Makri, N., and Miller, W. H., 1989, *J. chem. Phys.*, **91,** 4026.
[9] Sewell, T. D., Guo, Y., and Thompson, D. L., 1996, *J. chem. Phys.*, **103,** 8557.
[10] Guo, Y., and Thompson, D. L., 1996, *J. chem. Phys.*, **105,** 1070.
[11] Guo, Y., and Thompson, D. L., 1996, *J. chem. Phys.*, **105,** 7480.
[12] Guo, Y., Li, S., and Thompson, D. L., 1997, *J. chem. Phys.*, **107,** 2853.
[13] Siebrand, W., Wildman, T. A., and Zgierski, M. Z., 1984, *J. Am. chem. Soc.*, **106,** 4083, 4089.
[14] Smedarchina, Z., and Siebrand, W., 1993, *Chem. Phys.*, **170,** 347.
[15] Houk, K. N., Li, Y., McAllister, M. A., O'Doherty, G., Paquette, L. A., Siebrand, W., and Smedarchina, Z. K., 1994, *J. Am. chem. Soc.*, **116,** 10895.
[16] Miller, W. H., 1975, *J. chem. Phys.*, **62,** 1899.
[17] Benderskii, V. A., Goldanskii, V. I., and Makarov, D. E., 1993, *Phys. Rep.*, **233,** 195.
[18] Benderskii, V. A., Makarov, D. E., and Wight, C. H., 1994, *Adv. Chem. Phys.*, **88,** 1.
[19] Smedarchina, Z., Siebrand, W., Zgierski, M. Z., and Zerbetto, F., 1995, *J. chem. Phys.*,**102,** 7024.
[20] Smedarchina, Z., Caminati, W., and Zerbetto, F., 1995, *Chem. Phys. Lett.*, **237,** 279.
[21] Smedarchina, Z., Siebrand, W., and Zgierski, M. Z., 1995, *J. chem. Phys.*, **103,** 5326.
[22] Smedarchina, Z., Siebrand, W., and Zgierski, M. Z., 1996, *J. chem. Phys.*, **104,** 1203.
[23] Smedarchina, Z., Fernández-Ramos, A., and Rios, M. A., 1997, *J. chem. Phys.*, **106,** 3956.
[24] Smedarchina, Z., and Zerbetto, F., 1997, *Chem. Phys. Lett.*, **271,** 189.
[25] Fernández-Ramos, A., Smedarchina, Z., Zgierski, M. Z., and Siebrand, W., 1998, *J. chem. Phys.*, **109,** 1004.
[26] Smedarchina, Z., Zgierski, M. Z., Siebrand, W., and Kozlowski, P. M., 1998, *J. chem. Phys.*, **109,** 1014.
[27] Smedarchina, Z., Fernández-Ramos, A., Zgierski, M. Z., and Siebrand, W., 1998, DOIT 1.1, a computer program to calculate hydrogen tunnelling rate constants and splittings, National Research Council of Canada, http://www.sims.nrc.ca/sims/software/doit/index.html.
[28] Sekiya, H., Nagashima, Y., and Nishimura, Y., 1990, *J. chem. Phys.*, **92,** 5761.

[29] Sekiya, H., Nakomo, N., Nishi, K., Hamabe, H., Sawada, T., Tashiro, M., and Nishima, Y., 1995, *Chem. Lett.*, **1995,** 893.
[30] Al-Soufi, W., Grellmann, K. H., and Nickel, B., 1991, *J. phys. Chem.*, **95,** 10503.
[31] Eckart, C., 1935, *Phys. Rev.*, **47,** 552.
[32] Caldeira, A. O., and Leggett, A. J., 1983, *Ann. Phys.*, **149,** 374; Leggett, A. J., Chakravarty, S., Dorsey, A. T., Fischer, M. P. A., Garg, A., and Zwerger, M., 1987, *Rev. mod. Phys.*, **59,** 1.
[33] Grabert, H., Schramm, D. N., and Ingold, G. L., 1988, *Phys. Rep.*, **168,** 115.
[34] Silbey, R., and Harris, R. H., 1983, *J. chem. Phys.*, **78,** 2330.
[35] Affleck, I., 1981, *Phys. Rev. Lett.*, **46,** 388.
[36] Landau, L. D., and Lifshitz, E. M., 1981, *Quantum Mechanics* (Oxford: Pergamon).
[37] Feynman, R. P., and Hibbs, A. R., 1965, *Quantum Mechanics and Path Integrals* (New York: McGraw-Hill).
[38] Benderskii, V. A., Goldanskii, V. I., and Makarov, D. E., 1991, *Chem. Phys.*, **154,** 407.
[39] Goldanskii, V. I., 1959, *Dokl. Akad. Nauk*, **124,** 1261; 1959, *ibid.*, **127,** 1037; 1979, *Nature*, **279,** 109.
[40] Frisch, M. J., Trucks, G. W., Schlegel, H. B., Gill, P. M. W., Johnson, B. J., Robb, M. A., Cheeseman, J. R., Keith, T. A., Petersson, G. A., Montgomery, J. A., Raghavachari, K, Al-Laham, L. A., Zakrzewski, V. G., Ortiz, J. V., Foresman, J. B., Peng, C. Y., Ayala, P. Y., Chen, W., Wong, M. W., Andres, J. L., Replogle, E. S., Gomperts, R., Martin, R. L., Fox, D. J., Binkley, J. S., Defrees, D. J., Baker, J., Stewart, J. P., Head-Gordon, M., Gonzalez, C., and Pople, J. A., 1995, Gaussian 94, Revision B.3 (Pittsburgh PA: Gaussian, Inc.).
[41] Alves, A. C. P., Hollas, J. M., Musa, H., and Ridley, T., 1985, *J. molec. Spectrosc.*, **109,** 99; Redington, R. L., Chen, Y., Scherer, G. J., and Field, R. W., 1988, *J. chem. Phys.*, **88,** 627; Sekiya, H., Nagashima, Y., and Nishimura, Y., 1989, *Bull. chem. Soc. Jpn.*, **62,** 3229; Sekiya, H., Nagashima, Y., and Nishimura, Y., 1990, *J. chem. Phys.*, **92,** 5761.
[42] Bondybey, V. E., Haddon, R. C., and English, J. H., 1984, *J. chem. Phys.*, **80,** 5432.
[43] Baughcum, S. L., Smith, Z., Wilson, E. B., and Duerst, R. W., 1984, *J. Am. chem. Soc.*, **106,** 2260; Turner, P., Baughcum, S. L., Coy, S. L., and Smith, Z., 1984, *ibid.*. **106**, 2265.
[44] Bicerano, J., Schaefer, W. F., and Miller, W. H., 1983, *J. Am. chem. Soc.*, **105,** 2550.
[45] Carrington, T., and Miller, W. H., 1986, *J. chem. Phys.*, **84,** 4364.
[46] Shida, N., Barbara, P. F., and Almlof, J. E., 1989, *J. chem. Phys.*, **91,** 4061.
[47] Kato, S., Kato, H., and Fukui, K., 1977, *J. Am. chem. Soc.*, **99,** 684.
[48] Makri, N., and Miller, W. H., 1989, *J. chem. Phys.*, **91,** 7026.
[49] Bosch, E., Moreno, H., Lluch, J. M., and Bertran, J., 1990, *J. chem. Phys.*, **93,** 5685.
[50] Baughcum, S. L., Duerst, R. W., Rowe, W. F., Smith, Z., and Wilson, E. B., 1981, *J. Am. chem. Soc.*, **103,** 6296.
[51] Smith, Z., Wilson, E. B., and Duerst, R. W., 1983, *Spectrochim. Acta*, **39A,** 1117.
[52] Frost, R. K., Hagermeister, F. C., Arrington, C. A., Zwier, T. S., and Jordan, K. D., 1996, *J. chem. Phys.*, **105,** 2595.
[53] Borchardt, D. B., and Bauer, S. H., 1986, *J. chem. Phys.*, **85,** 4980.
[54] Carter, R. E., Drakenberg, T., and Bergman, N. A., 1975, *J. Am. chem. Soc.*, **97,** 6990.
[55] Bak, B., and Skaarup, S., 1971, *J. molec. Struct.*, **10,** 385.
[56] Deycard, S., Lusztyk, J., Ingold, K. U., Zerbetto, F., Zgierski, M. Z., and Siebrand, W., 1988, *J. Am. chem. Soc.*, **110,** 6721.
[57] Smedarchina, Z., and Fernández-Ramos, A., unpublished results.
[58] Deycard, S., Lusztyk, J., Ingold, K. U., Zerbetto, F., Zgierski, M. Z., and Siebrand, W., 1990, *J. Am. chem. Soc.*, **112,** 4284.
[59] Butenhoff, T. J., and Moore, C. B., 1988, *J. Am. chem. Soc.*, **110,** 8336.
[60] Braun, J., Schlabach, M., Wehrle, B., Kocher, M., Vogel, E., and Limbach, H.-H., 1994, *J. Am. chem. Soc.*, **116,** 6593.
[61] Braun, J., Limbach, H.-H., Williams, P. G., Morimoto, H., and Wemmer, D. E., 1996, *J. Am. chem. Soc.*, **118,** 7231.
[62] Sarai, A., 1982, *J. chem. Phys.*, **76,** 5554.
[63] Smedarchina, Z., Siebrand, W., and Wildman, T. A., 1988, *Chem. Phys. Lett.*, **143,** 395.
[64] Schlabach, M., Wehrle, B., and Limbach, H.-H., 1989, *Angew. Chem. Int. Ed. Engl.*, **28,** 76.

[65] SMEDARCHINA, Z., SIEBRAND, W., and ZERBETTO, F., 1989, *Chem. Phys.*, **136,** 285.
[66] BRAUN, J., SCHWESINGER, R., WILLIAMS, P. G., MORIMOTO, H., WEMMER, D. E., and LIMBACH, H.-H., 1996, *J. Am. chem. Soc.*, **118,** 11101.
[67] KOZLOWSKI, P. M., ZGIERSKI, M. Z., and PULAY, P., 1995, *Chem. Phys. Lett.*, **247,** 379.
[68] KOZLOWSKI, P. M., JARZECKI, A. A., PULAY, P., LI, X. Y., and ZGIERSKI, M. Z., 1996, *J. phys. Chem.*, **100,** 13985; KOZLOWSKI, P. M., JARZECKI, A. A., and PULAY, P., 1996, *J. phys. Chem.*, **100,** 7007.
[69] BENDERSKII, V. A., GOLDANSKII, V. I., and GRINEVICH, P. G., 1993, *Chem. Phys.*, **170,** 275.
[70] FERNÁNDEZ, B., and FERNÁNDEZ-RAMOS, A., to be published.
[71] SYAGE, J. A., 1993, *Chem. Phys. Lett.*, **202,** 227.
[72] SYAGE, J. A., 1995, *J. phys. Chem.*, **99,** 5772.
[73] KIM, S. K., BREEN, J. J., WILBERG, D. M., PENG, L. W., HEIKAL, A., SYAGE, J. A., and ZEWAIL, A. H., 1995, *J. chem. Phys.*, **99,** 7421.
[74] SIEBRAND, W., ZGIERSKI, M. Z., SMEDARCHINA, Z., VENER, M., and KANETI, J., 1997, *Chem. Phys. Lett.*, **266,** 47.
[75] SIEBRAND, W., ZGIERSKI, M. Z., and SMEDARCHINA, Z., 1997, *Chem. Phys. Lett.*, **279,** 377.
[76] SMEDARCHINA, Z., SIEBRAND, W., and ZGIERSKI, M. Z., unpublished results.
[77] GORDON, M. S., 1996, *J. phys. Chem.*, **100,** 3974.
[78] KEMBLE, E., 1935, *Phys. Rev.*, **48,** 549.